WHAT CAN PAIRED MEASUREMENTS OF Th ISOTOPE ACTIVITY AND PARTICLE CONCENTRATION TELL US ABOUT PARTICLE CYCLING IN THE OCEAN?

Olivier Marchal

Woods Hole Oceanographic Institution
Woods Hole, MA 02543, USA
Tel: +1 508 289 3374
Fax: +1 508 457 2187
email: omarchal@whoi.edu

Phoebe J. Lam

Woods Hole Oceanographic Institution
Woods Hole, MA 02543, USA

April 17, 2012

Abstract

The ability of paired measurements of thorium isotope activity and particle concentration to constrain rate constants of sorption reactions and particle dynamics in the ocean is examined. This study is motivated by GEOTRACES and other sampling programs where Th and particle data are gathered in various oceanic environments. Our approach relies on inversions with a model of trace metal and particle cycling in the water column. First, the model is used to simulate vertical profiles of (i) the activity of three Th isotopes (^{228,230,234}Th) in the dissolved phase, small suspended particles, and large sinking particles, and (ii) the concentration of small and large particles. The simulated profiles are then subsampled and corrupted with noise to generate a pseudo data set. These data are combined with the model with arbitrary values of rate constants of Th adsorption, Th desorption, particle sinking, particle remineralization, and particle (dis)aggregation in an effort to recover the actual values used to generate the data. Inversions are performed using a least-squares technique with varying assumptions about data noise, data sampling, and model errors.

We find that accurate and precise recovery of rate parameters is possible when all data have a relative error of less than 20%, vertical sampling is dense enough to resolve activity and concentration gradients, and model errors are negligible. Estimating cycling rates from data with larger errors and (or) at locations where model assumptions are not tenable would remain challenging. On the other hand, the paired data set would improve significantly the relative precision of rate parameters compared to that of prior estimates ($\geq$ 100%), even with current data uncertainties and significant model errors. Based on these results, we advocate the joint measurement of all three Th isotopes, ^{228}Ra, and particles collected by in situ filtration within GEOTRACES and other sampling programs targeted at the study of particle processes in the ocean.

1 INTRODUCTION

The production, transport, and destruction of particles in the ocean have profound consequences for the marine biogeochemical cycle of a wide range of constituents. For example, chemical elements such as nitrogen, phosphorous, and carbon are incorporated into the biogenic particles that are produced in the upper layers of the sea. These particles sink by gravity and tend to be decomposed at depth, leading to the release of these elements to the dissolved phase in deep water. This vertical transport of constituents by particle cycling is thought to strongly influence the large-scale distribution of a number of substances in the ocean, such as biological nutrients, dissolved oxygen, and dissolved inorganic carbon.

The exchange of chemical constituents between the dissolved phase and particles in the ocean can take different forms, including adsorption, desorption, (in)organic complexation, and biologically-mediated uptake and remineralization. Besides, ocean particles are subject to a wide variety of processes, such as precipitation, sinking, remineralization or dissolution, (dis)aggregation, and transport by currents. Present-day knowledge about sorption reactions and particle processes in the ocean stems largely from measurements of particle-reactive metals, in particular thorium. Estimates of rate constants of Th and particle cycling have been obtained from such measurements at various locations in the world oceans, e.g., in the North Pacific (*Nozaki et al.*, 1981; *Nozaki et al.*, 1987; *Murnane et al.*, 1990; *Clegg et al.*, 1991), the Equatorial Pacific (*Clegg et al.*, 1991), the Panama Basin (*Bacon and Anderson*, 1982), the Arctic Ocean (*Bacon et al.*, 1989; *Lepore and Moran*, 2007), the North Atlantic (*Cochran et al.*, 1993; *Murnane et al.*, 1994; *Murnane et al.*, 1996), the Ross Sea (*Cochran et al.*, 2000), the Indian Ocean near Kerguelen Islands (*Venchiarutti et al.*, 2008), and the Drake Passage (*Venchiarutti et al.*, 2011). These estimates range over several orders of magnitude and suffer generally from very large uncertainties (Figure 1): point estimates of the cycling rates range from 0.1 to 1 y^{-1} for adsorption, 1 to 10 y^{-1} for desorption, 10 to 100 y^{-1} for remineralization, 0.1 to 100 y^{-1} for aggregation, and 1 to 1000 y^{-1} for disaggregation. Likewise, estimates of the sinking speed of marine particles that have been derived from various methods span a large range and commonly lie between tens to a few hundred m d^{-1} (for a recent short review see *McDonnell and Buesseler* (2010). These very large uncertainties constitute a severe impediment to the description of biogeochemical processes in ocean models.

This paper explores the extent to which measurements of the activity of three Th isotopes (^{228,230,234}Th) can, in combination with measurements of particle concentration, constrain aspects of Th and particle cycling in the ocean. It is motivated by the extensive set of measurements obtained during GEOTRACES and other sampling programs concerned with particle-reactive substances. Among the overriding goals of GEOTRACES is the evaluation of sources, sinks, and internal cycling of selected trace elements and isotopes in the ocean (*GEOTRACES*, 2006). A major objective of this paper is to determine the extent to which the types of measurements gathered during GEOTRACES and other programs could provide accurate and precise estimates of the rate constants of Th and particle cycling in the deep sea. In particular, the sensitivity of the derived rate constants to the uncertainties in the Th and particle data is estimated, thereby providing a target for analytical improvements.

Our approach to reach the above objective is the following. First, a model that describes the cycling of trace metals and particles in the oceanic column is used to simulate the vertical distributions of ^{228,230,234}Th activity and particle concentration in different size fractions. The distributions of Th isotope activity and particle concentration calculated by the model are then subsampled and contaminated with noise in order to generate an idealized data set. These data are combined with the model with arbitrary values of the rate constants in an effort to recover the original values of the constants that have been used to generate the data. Since the values of the rate parameters used to generate the data are known exactly, the ability of the data to estimate these parameters can be tested. The approach described above is often referred to as 'twin experiments' in other contexts and is routinely applied to test data assimilation procedures.

An inverse method is used to combine the data of Th isotope activity and particle concentration with the model of trace metal and particle cycling. Accordingly, this investigation builds to a large extent upon prior work by R. Murnane and his colleagues, who extensively applied such methods to the study of thorium and particles in the ocean (*Murnane* *et al.*, 1990; *Murnane et al.*, 1994; *Murnane*, 1994; *Murnane et al.*, 1996). Our work shows both similarities and differences with these previous applications. The most significant difference is perhaps the absence of measurements of the vertical flux of Th isotopes and particles in the present study, since sediment traps are typically not deployed along transoceanic sections such as completed during GEOTRACES. On the other hand, measurements of particle concentration in different size fractions, which are lacking in previous applications, are considered here since such measurements are becoming more commonly available.

This paper is organized as follows. The model of trace metal and particle cycling, the idealized data, and the inverse method are described in section 2. In section 3, the ability of the data to recover rate constants in the presence of data errors, model errors, and (or) limited sampling is examined. Emphasis is placed on both the accuracy and the precision of the rate constants estimated by inversion. More specific aspects of the estimation problem and limitations of our approach are discussed in section 4. Conclusions follow in section 5.

2 METHODOLOGY

The methodology being used comprises three main components: a model that describes the cycling of trace metals and particles in the ocean, a set of idealized measurements, and an inverse method that combines the model with the measurements. The domain of investigation is supposed to represent the water column at a deep ocean station occupied during a large-scale sampling program such as GEOTRACES. It extends from the base of the euphotic zone (taken at $z_e = 110$ m) to the bottom ($z_b = 5000$ m). By restricting the domain to below the euphotic zone, particle production by photosynthesis does not need to be considered and a relatively simple model of particle cycling could be used. By convention, the vertical direction is pointing downwards.

2.1 Model of Trace Metal and Particle Cycling

2.1.1 Trace metal cycling

The model of trace metal cycling is a very simplified description of the behaviour of particle-reactive substances in the ocean (Figure 2). It is analogous to the model proposed by *Bacon et al.* (1985), with the addition of the remineralization of small particles leading to the release of small particulate material to solution (see below). The resulting model is identical to that applied in subsequent analyses of Th and particle measurements on oceanic samples (e.g., *Murnane et al.* (1990); *Cochran et al.* (1993); *Murnane et al.* (1994); *Murnane* (1994); *Murnane et al.* (1996); *Cochran et al.* (2000); *Lepore and Moran* (2007)). The interested reader is invited to consult these references for a discussion of the model assumptions.

In the model, the activity of each Th isotope (^{228}Th, ^{230}Th, and ^{234}Th) is divided in three phases: the dissolved phase, the small particles, and the large particles (Figure 2). These phases have the following operational definitions. The dissolved phase designates the material that passes through a conventional filter with a nominal porosity of about 0.5 μm. The small particle fraction refers to the material in the size range from about 0.5 μm to about 50 μm. This fraction can be sampled from water pumped by large volume filtration (LVF) and is assumed here to be suspended, i.e., it does not sink by gravity. Finally, the large particle fraction denotes the material with a size larger than about 50 μm. It can also be sampled by LVF and is assumed here to sink.

The specific processes being considered in the model include, for each Th isotope, the production by the radioactive parent, the radioactive decay, the adsorption onto small particles, the release from small particles by desorption and remineralization, the exchange between the small and large particles by particle (dis)aggregation, and the vertical transport due to the sinking of large particles. The processes associated with solution-solid exchange are assumed to follow first-order kinetics. Thus, the governing equations for the activity of each isotope in the dissolved phase (A_d, in dpm m^{-3}), the small particles (A_s, dpm m^{-3}), and the large particles (A_l, dpm m^{-3}) are

$$
\begin{aligned}
T(A_d) &= \lambda A_p + (k_{-1} + \beta_{-1}) A_s - (k_1 + \lambda) A_d, &\text{(1a)}\\
T(A_s) &= k_1 A_d + \beta_{-2} A_l - (k_{-1} + \beta_{-1} + \beta_2 + \lambda) A_s, &\text{(1b)}\\
T(A_l) &= \beta_2 A_s - (\beta_{-2} + \lambda) A_l - w\frac{\partial A_l}{\partial z}. &\text{(1c)}
\end{aligned}
$$

Here A_p is the activity of the radioactive parent, λ the radioactive decay constant, k_1 the adsorption rate, k_{-1} the desorption rate, β_{-1} the remineralization rate, β_2 the aggregation rate, β_{-2} the disaggregation rate, and w the particle sinking speed. The term $T(\cdot)$ includes the temporal rate of change as well as the effects of advection and diffusion, e.g., $T(A_d) = \partial A_d/\partial t + \mathbf{u} \cdot \nabla A_d - \nabla \cdot (\mathbf{K} \nabla A_d)$, where t is time, $\mathbf{u}$ the vector velocity, and $\mathbf{K}$ a diffusion tensor. Note that the different effects in $T(\cdot)$ are not represented in Figure 2. There is a system of equations (1a–1c) for each Th isotope, so the model of trace metal cycling comprises a total of nine equations.

The radioactive decay constants and the radioactive parent activities that are assumed in this work are listed in Table 1. The activity of ^{228}Ra (half-life of 5.7 y) shows generally large vertical variations in the ocean, with maxima near the surface and the bottom, and minima at mid-depth (e.g., *Key et al.* (1992)). Since ^{228}Ra is supplied from sediments, highest ^{228}Ra activities are observed in surface waters near the coasts and in bottom waters. In order to represent vertical variations of ^{228}Ra activity in our analysis, the ^{228}Ra activity is set to vary with depth according to:

$$
^{228}\mathrm{Ra}(z) = Ae^{-(z-z_e)/l_{\mathrm{Ra}}} + Be^{-(z_b-z)/l_{\mathrm{Ra}}}, \qquad (2)
$$

where $A = 30$ dpm m^{-3}, $B = 5$ dpm m^{-3}, and $l_{\mathrm{Ra}} = 500$ m. The vertical distribution of ^{228}Ra described by this equation exhibits an exponential decrease from the base of the euphotic zone (where $^{228}\mathrm{Ra} = 30$ dpm m^{-3}) and an exponential decrease from the bottom (where $^{228}\mathrm{Ra} = 5$ dpm m^{-3}), with much smaller activities at mid-depth (minimum of 0.2 dpm m^{-3} near $z = 3000$ m). In contrast to ^{228}Ra, the ^{234}U and ^{238}U activities are thought to exhibit relatively small variations in the ocean where uranium tends to vary linearly with salinity and hence to behave conservatively (e.g., *Owens et al.* (2011)). Here these activities are taken as vertically uniform. The ^{238}U activity is fixed at 2.4×10^3

dpm m^{-3} assuming a salinity of 35 (*Owens et al.*, 2011) and the ^{234}U activity is fixed at $2.4 \times 1.14 = 2.7 \times 10^3$ dpm m^{-3} assuming a ^{234}U/^{238}U ratio of 1.14 for seawater (*Chen et al.*, 1986; *Robinson et al.*, 2004).

In order to generate idealized Th data, equations (1a–1c) are solved for the Th isotope activity in each phase by making the following assumptions. First, the effects of unsteadiness, advection, and diffusion are assumed to be negligible in the Th isotope balances, i.e., $T(A_d) = T(A_s) = T(A_l) = 0$. These assumptions are unlikely to be valid for all Th isotopes and (or) at all oceanic locations. Vertical profiles of ^{230}Th at several locations in the North Pacific are consistent with a reversible exchange with settling particles and do not seem to require a significant influence of ocean circulation (e.g., *Nozaki et al.* (1981); *Roy-Barman et al.* (1996)). Measurements of ^{230}Th activity in the North Atlantic, however, have been suggested to reflect a significant effect of deep circulation (e.g., *Cochran et al.* (1987); *Moran et al.* (1997); *Vogler et al.* (1998); *Moran et al.* (2002); *Marchal et al.* (2007)). Second, the presence of a vertical derivative in (1c) implies that a boundary condition is required to solve the system (1a–1c). The derivative is present in the equation for large particle activity, so either the large particle activity or the flux of Th in large particles should be prescribed at a given depth. Here the large particle activity at depth z_e is fixed to 0.01 dpm m^{-3} for ^{228}Th, 0.001 dpm m^{-3} for ^{230}Th, and 2.5 dpm m^{-3} for ^{234}Th. These values are generally consistent with specific activities (dpm per particle mass) measured on material collected by sediment traps deployed in the upper 400 m at different locations in the North Atlantic (*Brewer et al.*, 1980; *Cochran et al.*, 1993; *Roy-Barman et al.*, 2005), assuming a concentration of large particles of 1×10^{-6} kg m^{-3} (see below). Finally, the rate constants k_1, k_{-1}, w, β_{-1}, β_2, and β_{-2} take on the values of Table 2 (3rd column), which are within the range of published estimates (Figure 1).

With the above assumptions, the Th isotope equations (1a–1c) reduce to a system of ordinary differential equations that can be solved exactly by Laplace transform. Note that equations (1a–1c) can be solved for the Th isotope activities independently of the concentrations of particles. This possibility arises from the fact that these activities are expressed in dpm per volume of water, since measured ^{228,230,234}Th activities, including particle activities derived from in situ filtration, are usually given in dpm per volume or mass of water. If the particle activities were expressed instead in dpm per mass of particles, then particle concentrations would appear explicitly in (1a–1c) and they should be known in order to determine the Th activities (the particle cycling model is described section 2.1.2).

The vertical distributions of Th isotope activity, which are obtained by analytical solution of (1a–1c), are displayed in Figure 3 to Figure 5 (solid lines). The activity of ^{228}Th in the dissolved phase and the small particles show maxima near the surface and the bottom, where the radioactive parent ^{228}Ra is relatively abundant (Figure 3). In contrast, the activity of ^{228}Th in the large particles presents a subsurface maximum, which reflects a balance between the effects of particle (dis)aggregation, radioactive decay, and particle sinking (equation 1c). The activity of ^{230}Th increases quasi-linearly with depth in each phase, which arises from the reversible exchange with particles and a relatively long half-life (Figure 4). Finally, the activity of the short-lived ^{234}Th shows, for each phase, a decrease in the upper 1000 m and nearly uniform values in the deeper part of the water column, where secular equilibrium with the progenitor ^{238}U is almost reached (Figure 5).

Albeit instructive, the analytical model described above would generally not be appropriate for combination with real measurements, as it neglects possible vertical variations of the rate constants. In order to allow for such variations, a numerical model is considered. Equations (1a–1c) are thus approximated with finite differences at grid points extending from the base of the euphotic zone to the bottom. The grid points of the numerical model belong to two subsets. The grid points of a first subset coincide with the fourteen deepest levels of a sampling scheme adopted at some of the stations occupied during the US GEOTRACES North Atlantic section (completed in 2010–2011): 110, 135, 185, 250, 550, 850, 965, 1500, 2100, 3000, 3600, 4300, 4750, and 4900 m. For convenience, stations with this sampling scheme are referred to below as ‘GEOTRACES NA deep stations’. The grid points of the second subset are intermediate points located between the sampling depths. Specifically, two additional points whose depth is found by linear interpolation are included between each pair of adjacent sampling depths. The addition of intermediate points between sampling depths increases the resolution of the numerical model and leads to accurate results (see below). The two subsets form a total of 40 grid points including the boundary point at $z_e = 110$ m where the large particle activities are prescribed. The sinking term $w\partial A_l/\partial z$ in (1c) is approximated by a central difference scheme at all points except at the deepest point ($z = 4900$ m) where it is approximated with backward differencing.

The vertical distributions of ^{228,230,234}Th, which are obtained numerically, are compared to those calculated analytically in order to test the accuracy of the numerical model (compare dashed lines with solid lines in Figure 3 to Figure 5). They rely on the same assumptions as for the analytical solution. The relative error in the Th isotope activities determined numerically is ≤ 0.01 on average for each Th isotope and for each phase, indicating that the numerical solution is accurate.

2.1.2 Particle cycling

The model of particle dynamics is a very crude description of the behaviour of particles in the ocean (Figure 2). It is similar to the model proposed and applied by *Clegg and Whitfield* (1990), *Clegg and Whitfield* (1991), and *Clegg et al.* (1991), except that the production of small particles and the remineralization of large particles are disregarded. It is identical to the model adopted in previous inversions of Th and particle data (*Murnane et al.*, 1990; *Murnane et al.*, 1994; *Murnane*, 1994; *Murnane et al.*, 1996). A critical discussion of the model assumptions was recently provided by *Burd and Jackson* (2009). For example, whereas the model assumes first-order kinetics for particle processes, aggregation is thought as a second-order process that involves the collision of two particles, leading to a different interpretation of the rate constant for aggregation in the model.

In the model, the concentration of particles is considered only in two size classes: the small particles and the large particles (Figure 2). The processes being considered are the aggregation of small particles to form large particles, the remineralization of small particles, the disaggregation of large particles into small particles, and the sinking of large particles. The governing equations for particle concentration in the small size fraction (P_s, in kg m^{-3}) and large size fraction (P_l, kg m^{-3}) are thus

$$T(P_s) = \beta_{-2} P_l - (\beta_{-1} + \beta_2) P_s, \quad (3a)$$
$$T(P_l) = \beta_2 P_s - \beta_{-2} P_l - w \frac{\partial P_l}{\partial z}. \quad (3b)$$

In order to generate idealized particle data, equations (3a–3b) are solved for the vertical distributions of P_s and P_l by making assumptions similar to those for the Th isotopes. First, the effects of unsteadiness, advection, and diffusion are assumed to be negligible i.e., $T(P_s) = T(P_l) = 0$. Second, the presence of a vertical derivative in (3b) implies that a boundary condition is required to solve the particle equations (3a–3b), as for the Th equations. Since the derivative occurs in the equation for large particles, either the concentration or the flux of large particles should be imposed at a given depth. Here the concentration of large particles at depth z_e is fixed at $P_l = 1 \times 10^{-6}$ kg m^{-3}. This value can be derived, for example, from (i) a vertical particle flux of 100 mg m^{-2} d^{-1} at this depth, which compares favorably with the particle flux intercepted over most of the year by a sediment trap at 150 m in the Sargasso Sea (*Lohrenz et al.*, 1992), and (ii) a sinking velocity of large particles of 100 m d^{-1}. Finally, the rate constants w, β_{-1}, β_2, and β_{-2} take on the values that are listed in Table 2 (3rd column).

The vertical distributions of P_s and P_l, which are obtained by solving equations (3a–3b) analytically, show maxima near the surface and an exponential decrease with depth (solid lines in Figure 6). The length scale characterizing the exponential decrease of particle concentration is equal to $w(\beta_{-1}+\beta_2)/\beta_{-1}\beta_{-2}$ and is therefore the same for the two particle fractions. The ratio of small particle concentration to large particle concentration is given by $\beta_{-2}/(\beta_{-1} + \beta_2)$ and is thus the same at all depths.

Note that the decrease with depth of the concentration of particulate organic carbon (POC) measured on material collected by LVF has been described with a power law, not with an exponential function (*Lam et al.*, 2011). However, the POC decrease takes place primarily through the mesopelagic zone (between approximately 100 and 1000 m). In the abyssal region, which is the focus of this study (section 2.2.1), the difference between a power law and an exponentional function to describe the vertical distribution of particle concentrations should be relatively slight.

The vertical distributions of P_s and P_l obtained numerically using the same grid and finite-differencing as for the model of trace metal cycling are compared to the analytical solution (compare dashed lines with solid lines in Figure 6). The relative error in the particle concentrations determined numerically averages to less than 0.01, indicating good accuracy of the numerical solution.

2.1.3 Model errors

The assumption of vanishing model errors when inferring rate parameters from field measurements is likely to be generally unrealistic. Indeed, a variety of processes that are poorly or not represented in models of trace metal and particle cycling may significantly influence the Th isotope activities and (or) particle concentrations that are observed in situ (such processes include, for example, mesoscale eddies; *Sweeney et al.* (2003)). When such an influence is suspected, the model equations should not be imposed exactly in the data analysis. Moreover, model errors should include uncertainties in the radioactive sources λA_p (equation 1a), since these are never known perfectly. In particular, ^{228}Ra measurements at mid-depth can suffer from significant uncertainties, implying that the radioactive source and hence the equation for dissolved ^{228}Th should not be imposed too strictly in the analysis.

Different approaches to constrain model errors have been adopted in previous inversions of Th and particle measurements on oceanic samples (e.g., *Murnane et al.* (1994); *Murnane et al.* (1996)). In some inversions, model errors were assumed to be proportional to a prior estimate of the sum of the source, sink, and sinking terms (where present) in the Th and particle equations (*Murnane et al.*, 1994). In other inversions, based on time-series of data, model errors were taken as proportional to the standard deviation of the trends observed in the data (*Murnane et al.*, 1996). In the present analysis, where the data do not occur in the form of time series, the former approach to constrain model errors is adopted (section 2.3.2).

2.2 Idealized Data Set

The vertical distributions of Th isotope activity and particle concentration, which are computed from the numerical model (Figures 3–6), are used to produce an idealized data set from which the ability of Th and particle data to estimate cycling rates could be tested. This data set includes (i) the activity of ^{228}Th, ^{230}Th, and ^{234}Th in the dissolved phase, the small particles, and the large particles, and (ii) the particle concentration in the small and large size fractions. They would represent the types of measurement available at stations occupied during modern sampling programs, such as at the GEOTRACES NA deep stations. The types of measurement and the measurements errors, which are considered here, are specific to the US GEOTRACES North Atlantic plans and investigators, although they may apply to other programs as well. Two limitations need to be considered: the relatively limited number of samples and the presence of non-negligible uncertainties in the data.

2.2.1 Limited sampling

The Th isotope activities and particle concentrations will not be measured on all size fractions and at all pumping depths at GEOTRACES NA deep stations. The set of measurements that is considered to be available in this study is consistent with current expectations for the samples collected at these stations, although it is perhaps too optimistic (section 4.2). Specifically, the following data set is assumed to be available: (i) ^{228}Th for all size fractions and at all depths, (ii) $^{230}\mathrm{Th}_d$ at all depths, (iii) $^{230}\mathrm{Th}_s$ at the ten deepest levels (in our analysis, at $z \geq 550$ m), (iv) $^{230}\mathrm{Th}_l$ at a single depth (2100 m), (v) $^{234}\mathrm{Th}_d$ and $^{234}\mathrm{Th}_s$ at all depths, (vi) $^{234}\mathrm{Th}_l$ in the upper 500–1000 m ($z \leq 965$ m), and (vii) P_s and P_l at the ten deepest levels ($z \geq 550$ m), as for $^{230}\mathrm{Th}_s$. The following procedure is adopted to assign activity and concentration values at the model grid points, unless stipulated otherwise. The Th isotope activities and particle concentrations at grid points coinciding with measurement depths are the values derived from the numerical solution at these depths. The activities and concentrations at points between measurement depths are obtained by linear interpolation of these values. The activities and concentrations at all other points are obtained by extrapolation from the values derived numerically at the closest measurement depth (for example, $^{230}Th_l$ values above and below 2100 m are set equal to the value at 2100 m).

The number of data used in our analysis is further reduced for the following reason. Testing the ability to recover rate parameters from the present approach requires an assumption about their actual vertical distribution in the ocean. Rate parameters of sorptive reactions and particle cycling are likely to vary with depth, in particular in the mesopelagic zone. For example, the concentration of strong organic ligand in particulate matter (PM), as determined from the amount of Th adsorbed onto PM in 0.1 M HCl, was found to decrease with depth between 100 and 1000 m in the South Pacific and South Atlantic (*Hirose et al.*, 2011). Chemical and biological processes modify the physical properties of aggregates as they sink, thereby altering their settling speed (*Burd and Jackson*, 2009). The settling speed of particles has been estimated to increase by a factor of two between 100 and 2000 m and by 15–60% between 2000 and 3500 m at two stations in the Equatorial Pacific Ocean and the Arabian Sea (*Berelson*, 2002). Rates of particle sinking have also been inferred to increase with depth off Cape Blanc in the Eastern North Atlantic (*Fischer and Karakaş*, 2009). The rate constant for particle remineralization would decrease with depth as particles would comprise less labile material as they settle (for a review about particle degradation see *Boyd and Trull* (2007)). Likewise, processes responsible for particle (dis)aggregation (*Burd and Jackson*, 2009), such as zooplankton feeding and fecal pellet production, are likely to vary in intensity with depth.

For simplicity, our analysis is restricted to the abyssal region at depths $\geq$ 965 m (the deepest level where $^{234}Th_l$ might be measured at GEOTRACES NA deep stations). Accordingly, only the data occurring at depths $\geq$ 965 m are used to recover the rate parameters by inversion. Furthermore, the rate parameters to be recovered from Th and particle data are taken as vertically uniform in the abyssal region, unless stated otherwise. Note that the assumption of uniform cycling rates even at abyssal depths cannot be rigorously defended. It would certainly not be valid at all oceanic locations. For example, the presence of a benthic nepheloid layer can lead to variations in at least some of the rate constants, as discussed in section 4.1. In that section, the estimation of a nonuniform rate parameter from Th and particle data is addressed.

2.2.2 Data errors

Uncertainties in the measurements of Th isotope activity and particle concentration on oceanic samples arise from various sources, such as inadequate sample volumes, imperfections in sample collection, preservation, and preparation, and instrumental errors. The relative errors for the measurements of Th isotope activity and particle concentration, which are assumed in this work, are listed in Table 3. The relative error of 15% for ^{228}Th measured on the dissolved phase and the small particles is within the expected range of uncertainty (M. Charette, pers. comm.). The relative error of 20% for ^{230}Th measured on these fractions is an assessment by the present authors based on results from an intercalibration coordinated by GEOTRACES (plots kindly provided by R. Anderson). Measurements of ^{228}Th and ^{230}Th on large particles have rarely or never been attempted and are arbitrarily assumed here to have a relative error of 50%. Although samples from multiple depths may need to be combined in order to exceed the detection limits of instruments (M. Charette, pers. comm.), combination of multiple samples is not considered in our analysis. The errors in ^{234}Th measurements are relatively small due to the abundance of ^{234}Th in seawater compared to that of ^{228}Th and ^{230}Th. The relative error of 5% for ^{234}Th measured on each fraction (Table 3) is consistent with published estimates (e.g., *Buesseler et al.* (2008)). Finally, a relative error of 20% is assumed for particle concentrations measured on water samples collected by LVF.

In order to account for measurement errors, the Th isotope activities and particle concentrations obtained from the numerical solution are corrupted with noise. The addition of noise requires an assumption about the underlying probability distributions of the activities and concentrations. If a normal (gaussian) probability distribution is assumed, the addition of noise can lead to negative values, which is unrealistic. Negative values are most likely to occur for measurements with the largest relative errors (Table 3). In order to avoid the occurrence of negative values, the Th isotope activities and the particle concentrations are assumed to follow lognormal distributions (*Aitchison and Brown*, 1957). For example, the ^{228}Th activity in the dissolved phase is, in the presence of measurement errors, set equal to

$$^{228}\mathrm{Th}_d' = e^{\mu + r\sigma}, \tag{4}$$

where

$$\mu = \ln\left(^{228}\mathrm{Th}_d\right) \qquad \text{and} \qquad \sigma = \sqrt{\ln\left(1 + \epsilon^2[^{228}\mathrm{Th}_d]\right)}. \tag{5}$$

Here $^{228}\mathrm{Th}_d$ is the value obtained from the numerical solution and (when applied) subsequent interpolation or extrapolation, and $\epsilon[^{228}\mathrm{Th}_d] = 0.15$ is the relative error in $^{228}\mathrm{Th}_d$ measurement (Table 3). The quantity r in (4) is a normal deviate with zero mean and unit variance, which is generated randomly. If a large number of values of r is generated for fixed $^{228}\mathrm{Th}_d$ and $\epsilon[^{228}\mathrm{Th}_d]$, the probability distribution of $^{228}\mathrm{Th}_d'$ tends to a lognormal distribution with median μ and variance σ^2. A test ensures that the values of $^{228}\mathrm{Th}_d'$ that are derived randomly are within $1 \pm \epsilon[^{228}\mathrm{Th}_d]$ of the value of $^{228}\mathrm{Th}_d$. The above procedure is applied to the other Th isotope activities and to the particle concentrations in all fractions. The Th and particle values at sampling depths, which are used to produce the idealized data for the inversions, are displayed together with their respective errors in Figure 3 to Figure 6 (open and solid circles, with horizontal bars).

2.3 Inverse Method

An inverse method is used to combine the model of trace metal and particle cycling (section 2.1) with the (idealized) measurements of Th isotope activity and particle concentration (section 2.2). This combination will inform us about the extent to which these types of measurement could be used to recover the rate constants k_1, k_{-1}, w, β_{-1}, β_2, and β_{-2} in the abyssal region (below a depth of 965 m). Since the measurements have significant errors, they should not be imposed exactly when inferring the rate constants. Here, the Th isotope activities and particle concentrations are, in addition to the rate constants, considered to be actually part of the solution. This approach allows the values of Th isotope activity and particle concentration to adjust in the inversions, while remaining consistent with the observed values. In order to avoid the inference of negative values, the inverse method aims at estimating, not the actual values, but their natural logarithm (e.g., *Murnane et al.* (1994)).

2.3.1 Algorithm of total inversion

The inverse method being used is a generalized least-squares method known as the algorithm of total inversion (*Tarantola and Valette*, 1982a; *Tarantola and Valette*, 1982b). A brief description of this method allows us to introduce concepts that are referred to later in the paper (for details see the above references). Let us first introduce a state vector $\mathbf{x}$ of dimension n. The components of $\mathbf{x}$ are the natural logarithm of (i) the activity of ^{228}Th, ^{230}Th, and ^{234}Th in the dissolved phase, the small particles, and the large particles, (ii) the particle concentration in the small and large size fractions, and (iii) the rate constants k_1, k_{-1}, w, β_{-1}, β_2, and β_{-2}, at different depths. The components of $\mathbf{x}$ represent the actual, true values to be estimated by inversion. If the number of depths where the components are to be estimated is m, then the dimension of $\mathbf{x}$ is $n = (3 \times 3 + 2 + 6)m = 17m$.

Let us then consider an a priori estimate of $\mathbf{x}$, which is noted $\mathbf{x}_o$. This prior estimate of the solution is obtained from the measurements of Th isotope activity and particle concentration (section 2.2) and from values of rate constants that are consistent with published estimates (Figure 1). Here the prior values of the rate constants are set equal to 5 ± 5 y^{-1} for both k_1 and k_{-1}, 300 ± 150 m d^{-1} for w, 10 ± 50 y^{-1} for β_{-1}, 10 ± 100 y^{-1} for β_2, and 500 ± 5000 y^{-1} for β_{-2} (Table 2, 4th column). The ranges defined by these values encompass most of the point estimates of these parameters in the ocean (Figure 1).

Let us then define a $n \times n$ error covariance matrix $\mathbf{C}_o$. The diagonal elements of $\mathbf{C}_o$ are the variances (standard deviations or errors squared) of the prior estimates in $\mathbf{x}_o$ and the off-diagonal elements of $\mathbf{C}_o$ are the covariances between these errors. Assuming that the Th activities, particle concentrations, and rate constants are lognormally distributed, the variances are set equal to $\ln(1+\epsilon^2[\cdot])$, where $\epsilon[\cdot]$ is the relative error for these variables (e.g., $\epsilon[k_1] = 5/5 = 1$). On the other hand, the covariances are set to zero, i.e., $\mathbf{C}_o$ is assumed to be diagonal.

Finally, let us consider the equations of the model of Th cycling (1) and particle dynamics (3), but with the trend and transport terms set equal to zero ($T(\cdot) = 0$). The finite-difference approximations that result from the discretization of these equations on the grid are included in a vector $\mathbf{f}(\mathbf{x}) = \mathbf{0}$. Thus, the vector $\mathbf{f}(\mathbf{x})$ includes the finite-difference forms of the source, sink, and sinking terms in equations (1) and (3). Its dimension is equal to $(3 \times 3 + 2)m = 11m$. The sinking terms are approximated with central differences at all interior points. The boundary points where large particle activities and concentrations are prescribed occur at $z = 965$ m and 4900 m. As for the data, the equations $\mathbf{f}(\mathbf{x}) = \mathbf{0}$ should not be imposed exactly when inferring rate constants in the ocean, since these equations contain uncertainties due to the assumption of steady state, the neglect of the effect of ocean circulation, the truncation error introduced by the numerical approximation of the sinking term, etc. Consequently, an error covariance matrix is also introduced for $\mathbf{f}(\mathbf{x}) = \mathbf{0}$, and noted $\mathbf{C}_f$. The diagonal elements of $\mathbf{C}_f$ are the square of the errors of the components of $\mathbf{f}(\mathbf{x})$, i.e., the square of the errors in the difference forms of the model equations. The off-diagonal elements of $\mathbf{C}_f$ are the covariances between these errors and are set equal to zero.

The problem considered in this paper is to find estimates of Th isotope activity, particle concentration, and rate constants k_1, k_{-1}, w, β_{-1}, β_2, and β_{-2}, which are consistent with (i) prior estimates of all these quantities and (ii) a model of trace metal and particle cycling. Equivalently, the problem is to find an estimate of $\mathbf{x}$ that is consistent with both the prior estimate $\mathbf{x}_o$ and the model equations $\mathbf{f}(\mathbf{x}) = \mathbf{0}$, given estimates of their respective errors. It is solved by determining a minimum of the objective function

$$J = (\mathbf{x} - \mathbf{x}_o)^T \, \mathbf{C}_o^{-1} \, (\mathbf{x} - \mathbf{x}_o) + \mathbf{f}(\mathbf{x})^T \mathbf{C}_f^{-1} \mathbf{f}(\mathbf{x}), \tag{6}$$

where the superscript ^{T} denotes the transpose. The first and second terms on the right-hand side describe, respectively, the deviation from the prior estimates and the deviation from the model equations. Since $\mathbf{C}_o$ and $\mathbf{C}_f$ are approximated by diagonal matrices, the objective function is a weighted sum of squares:

$$J = \sum_{i=1}^{17m} \left(\frac{x_i - x_{o,i}}{\sigma_{o,i}} \right)^2 + \sum_{i=1}^{11m} \left(\frac{f_i(\mathbf{x})}{\sigma_{f,i}} \right)^2, \tag{7}$$

where $\sigma_{o,i}$ is the standard deviation for the ith component of $\mathbf{x}_o$ and $\sigma_{f,i}$ is the standard deviation for the ith component of $\mathbf{f}(\mathbf{x}) = \mathbf{0}$. The matrices $\mathbf{C}_o$ and $\mathbf{C}_f$ play therefore the role of weighting factors, such that prior estimates or model equations with relatively large uncertainties contribute only modestly to the objective function to be minimized. For example, the relative errors $\geq 100\%$ for the prior estimates of the rate constants (Table 2) imply that the posterior estimates of these constants to be found by inversion may strongly deviate from the prior estimates (indeed, by one order of magnitude or more).

Note that the search for a minimum of J is a nonlinear problem, since the equations $\mathbf{f}(\mathbf{x}) = \mathbf{0}$ contain products of elements of $\mathbf{x}$ (e.g., $k_1\,{}^{228}\mathrm{Th}_d$ in equation (1a)): if the Th and particle data were to contain no error, then they could be taken as constant values and moved out of the state vector $\mathbf{x}$. In this case, the equations $\mathbf{f}(\mathbf{x}) = \mathbf{0}$ could be written as $\mathbf{Ax} = \mathbf{b}$, where $\mathbf{A}$ is a matrix of coefficients constrained from the data, $\mathbf{x}$ a vector of unknowns containing the rate constants, and $\mathbf{b}$ a vector including, e.g., the production rates from the radioactive parents. The search for a minimum of J would then reduce to a linear problem. The general validity of this approach, however, is doubtful for real (and thus uncertain) observations.

The method of total inversion is iterative in nature and proceeds by successive linearization of the nonlinear equations using their gradient with respect to the state vector. Accordingly, convergence of the method is only ensured if the nonlinearity is not too strong (*Tarantola and Valette*, 1982a). Here the algorithm is initialized with the prior estimate of the state, $\mathbf{x}_o$, and iteration is stopped when all the elements of the solution differ by less than 1% from those of the solution at the previous iterative step.

When a solution is found, the posterior estimates of the rate constants and their errors are derived as follows. The posterior estimates are obtained from the antilog of the solution elements (e.g., the posterior estimate of k_1 is obtained from the antilog of $\widehat{\ln k_1}$, where $\widehat{\ln k_1}$ is the estimate of the logarithm of k_1 that is found by inversion). If a solution element is the mean value of a normal distribution, then its antilog would be the median value of a lognormal distribution. Alternately, the posterior estimates of the rate constants can be derived using the formula for the mean of a lognormal random variable. For example, the posterior estimate of the adsorption rate, $\widehat{k_1}$, can be obtained from $\exp\left(\widehat{\ln k_1} + \sigma^2_{\widehat{\ln k_1}}/2\right)$, where $\sigma_{\widehat{\ln k_1}}$ is the error in the posterior estimate of $\ln k_1$ (*Aitchison and Brown* (1957); p. 8, equation 2.7). If nonlinearity is not too strong, the error $\sigma_{\widehat{\ln k_1}}$ can be derived using the formula for the error covariance matrix of the solution for the linear case (*Tarantola and Valette*, 1982a). The two forms (median and mean) of posterior estimate of the rate constants are considered here, as in previous inversions of Th and particle data (e.g., *Murnane et al.* (1994)).

Finally, the errors in the posterior estimate of the rate constants are computed using the formula for the standard deviation of a lognormal random variable (*Aitchison and Brown* (1957); p. 8, equation 2.8). For example, for the adsorption rate k_1,

$$\sigma^2_{\widehat{k_1}} = \exp\left(\sigma^2_{\widehat{\ln k_1}} + 2\widehat{\ln k_1}\right)\left(\exp\left(\sigma^2_{\widehat{\ln k_1}}\right) - 1\right). \tag{8}$$

In summary, the number of depths where the rate constants k_1, k_{-1}, w, β_{-1}, β_2, and β_{-2} are to be estimated from the Th and particle data amounts to $m = 20$ (six sampling depths plus fourteen intermediate depths between $z = 965$ m and 4900 m excluded). Consequently, the number of unknowns (size of $\mathbf{x}$) is 340 and the number of equations (size of $\mathbf{f}$) is 220. The inference of the rate constants is a formally underdetermined (and nonlinear) problem.

2.3.2 Prescription of model errors

Based on some of the concepts of the inverse method, the prescription of model errors in our analysis can be described precisely. Following a previous approach (*Murnane et al.*, 1994), the model errors are assumed to be proportional to the prior estimate of the sum of the source, sink, and sinking terms in the Th and particle equations:

$$\{\mathbf{C}_f\}_{i,j} = p\,\delta_{i,j}\{\mathbf{f}(\mathbf{x}_o)\mathbf{f}(\mathbf{x}_o)^T\}_{i,j}, \tag{9}$$

where $\{\cdot\}_{i,j}$ is the i, j element of the matrix, p is a proportionality factor, and $\delta_{i,j} = 1$ if $i = j$ and $\delta_{i,j} = 0$ if $i \neq j$. For example, the assumption $p = 1$ is equivalent to the statement that processes that are not represented explicitly in the model can be on the same order of magnitude as the prior estimate of the sum of the source, sink, and sinking terms.

3 RESULTS

In this section, the Th and particle data are combined with the model of Th and particle cycling to test the ability of these data to recover the rate parameters of the model. Emphasis is placed on the accuracy and precision with which the rates of adsorption, desorption, sinking, remineralization, and (dis)aggregation can be estimated. Results from a variety of inversions are reported in order to isolate the effects, on parameter recovery, of data errors, model errors, and limited sampling. Hypothetical cases where data or model errors are small or even zero and where data are available at all depths are considered first. We then examine more realistic cases where the uncertainty and availability of data approach those at stations occupied during modern sampling programs and where the model contains significant errors.

3.1 Effect of Data Errors

We first consider two different inversions where the Th and particle data have small uncertainties, they are available at all depths (no data interpolation or extrapolation is applied), and model errors are very small ($p = 10^{-5}$). Although these conditions are unlikely to be met in any real circumstances, the results from these inversions provide a useful reference as more realistic assumptions about the measurements and the model will be considered.

In a first inversion, the relative error of all data is fixed to 5%, which is comparable to the relative error of ^{234}Th measurements (for convenience this inversion is referred to below as our 'reference inversion'). It is seen that the rate parameters can all be successfully recovered in this case (solid circles in Figure 7). The posterior estimates of these parameters are close to the actual values used to generate the Th and particle data, and their posterior errors are small. This result indicates that accurate and precise recovery of the kinetic parameters from Th and particle data is a theoretical possibility. The Th and particle data overdetermine effectively the problem, so that all a priori information about the rate constants can be neglected. In this case, the iteration of the linearized problem always leads to the correct solution (*Tarantola and Valette*, 1982a).

In the second inversion, the relative error of all data is raised to a maximum of 20%, a value that seems to approximately hold for ^{230}Th measurements on the dissolved and small particle fractions. Thus, all measurements have the relative errors listed in Table 3, except ^{228}Th and ^{230}Th measurements on large particles whose relative error is 20%. As in the previous inversion, the prior estimates of the rate constants are adjusted so as to jointly satisfy the data and the model equations given their respective uncertainties (open circles in Figure 7). As expected, the recovery of the rate constants is generally poorer than in the previous case where data have a relative error of 5%, except for the adsorption rate that is still estimated with high accuracy and precision. The estimated rate constants are generally larger than those derived in this previous case. This pattern is due to the fact that inversions with larger data errors are less strongly influenced by Th and particle data and more strongly influenced by prior estimates of the rate constants (equation 7). Accordingly, since the prior estimates of the rate constants are set to be greater than their actual values, the posterior estimates of the rate constants obtained by inversion increase with the errors in the data. Nonetheless, most of the posterior estimates of the cycling rates are considerably more precise than the prior estimates, while being generally within one standard deviation of the actual values. This result suggests that Th and particle data with a relative error $\leq 20\%$ may still dramatically improve our understanding of solid-solution exchange and particle processes. Of course, this conclusion would hold only at locations where the data are available with good vertical resolution and the model provides an accurate description of Th and particle cycling (the effects of model errors and data resolution are explored later in sections 3.2 and 3.3, respectively).

A set of inversions illustrates more comprehensively the effect of varying data errors on the accuracy and precision of the recovered rate parameters (Figures 8–9). All these inversions assume that the data are available at all depths and that model errors are very small ($p = 10^{-5}$). The accuracy of a rate constant is measured by the normalized difference $(\hat{x} - x)/x$, where $\hat{x}$ is the value of the rate constant estimated by inversion (here the mean) and x is its actual value ($x \in \{k_1, k_1, w, \beta_{-1}, \beta_2, \beta_{-2}\}$). The precision is measured by the ratio $\sigma_{\hat{x}}/\hat{x}$, where $\sigma_{\hat{x}}$ is the standard deviation of rate constant x estimated by inversion (equation 8). As expected, both the accuracy and the precision of the recovered rate parameters deteriorate as the Th and particle data contain larger errors (Figures 8–9). Nonetheless, parameter recovery with $|\hat{x} - x|/x < 1$ and $\sigma_{\hat{x}}/\hat{x} < 1$ remains generally possible even in the presence of significant data errors (maximum of 20%). As already illustrated, not all parameters can be recovered with the same accuracy and precision: in general, the rate of Th adsorption onto small particles (k_1) and the rate of Th desorption from small particles (k_{-1}) are the parameters that are the easiest to infer from Th and particle data.

Note that, so far, the relative errors listed in Table 3 have been assigned to some but not all Th and particle data. Specifically, ^{228}Th and ^{230}Th measurements on large particles have been assumed to have a relative error of less than 50%. The case where the relative error in these measurements is equal to this value is examined in section 3.4.

3.2 Effect of Model Errors

As suggested above, the assumption of vanishing model errors when inferring rate constants from field data should generally be discouraged. In order to isolate the effect of model errors, inversions are considered where the Th and particle data are assumed to be perfect ($\sigma_o = 0$ for these data) and available at all depths. Note that the situation $\sigma_o = 0$ for some variables does not lead to infinite values in the algorithm of total inversion, as equation (7) may suggest. Indeed, the algorithm can rely on either $\mathbf{C}_o$ or its inverse through the use of a matrix identity (e.g., *Liebelt* (1967)).

The rate parameters that are estimated in two inversions with $p = 0.1$ or $p = 1$ are compared in Figure 10. It is seen that the second, more conservative assumption about the model ($p = 1$) leads to a significant deterioration of the accuracy and precision of the rate constants compared to the first assumption. In the second inversion, the rate constants are adjusted generally to a lesser degree from their prior estimates, which is consistent with a lower weight given to the model equations and, consequently, to the Th and particle data. On the other hand, the rate constants estimated by inversion are much more precise than the prior estimates (except for k_{-1} and w), while being within two standard deviations of the actual values. This result suggests that important information about the cycling rates could be extracted from Th and particle data even at locations where significant model errors should be assumed, provided that these data are accurate and numerous.

3.3 Effect of Limited Sampling

The above inversions assumed that Th and particle data are available at each depth of the model grid, i.e., at twenty two depths (8 sampling depths plus 14 intermediate depths between 965 and 4900 m included). No data interpolation or extrapolation was applied. In order to explore the effect of limited sampling, two other inversions are considered. In a first inversion, Th and particle data are assumed to be available at all depths and to contain no error. In the second inversion, the Th and particle values at levels between sampling depths are obtained by interpolation or extrapolation of the data at the sampling depths (section 2.1.1). Thus, for example, the values of ^{230}Th and ^{234}Th activity for large particles are extrapolated from their values at $z = 2100$ m and 965 m, respectively. The relative error of the data is fixed to 0% at the sampling and interpolation depths, and to 100% at the extrapolation depths. Both inversions assume that the model provides an accurate description of Th and particle cycling ($p = 0.01$).

We find that the rate parameters can still be recovered even with an incomplete data set, although the accuracy and precision of the posterior estimates vary between the rate constants and between different depths (Figure 11). This result suggests that the sampling scheme considered here (section 2.1.1) should be adequate for a successful estimation of cycling rates, provided that the data and the model are both accurate. This conclusion, however, should by tempered by the fact that the Th isotope activities and particle concentrations could exhibit, at some oceanic locations, much larger vertical gradients than in our synthetic data set (Figures 3–6). Indeed, no successful recovery of rate parameters should be anticipated at locations where sampling is not dense enough to resolve the property gradients.

3.4 Recovery of Cycling Rates at a Deep Ocean Station

The rates of Th and particle cycling are now estimated in the presence of data errors, model errors, and limited sampling. The errors in the Th and particle data that are anticipated for samples collected at GEOTRACES NA deep stations (Table 3) and the set of measurements that may be expected at these stations (section 2.2.1) are considered to provide a realistic example. Specifically, the relative errors at measurement depths are the values listed in Table 3. The relative errors at the interpolation points are given the same values, whereas the relative errors at the extrapolation points are set equal to 100%. The errors in the Th and particle equations are assumed to be on the order of the prior estimate of the sum of the source, sink, and sinking terms in these equations ($p = 1$). Note that whether this assumption would be generally valid when applied to the analysis of real data is unclear. For example, the prior estimate of the source, sink, and sinking terms at a given location may be very poor due to the currently large uncertainties in the rate parameters.

As expected from our previous inversions, the presence of significant errors both in the data and in the model decreases considerably the ability to recover the rate constants (Figure 12). Accurate and precise estimation of the cycling rates would remain challenging even with a relatively exhaustive data set, unless data errors are reduced and the assumption of small model errors is justified. Nevertheless, the posterior estimates of the rate constants would constitute a significant improvement over the prior estimates, in the sense that they would be generally much more precise (with the exception of k_{-1} and w), while being within two standard deviations of the actual values (Figure 13). When averaged over all depths in the abyssal region, the relative precision of the kinetic parameters (as measured by $\sigma_{\hat{x}}/\hat{x}$) is improved by about a factor of two for adsorption, four for remineralization and aggregation, and seven for disaggregation.

It is instructive to compare these results with those obtained from simpler approaches to infer rate constants of Th and particle cycling. Consider first the particle settling speed that would be inferred solely from ^{230}Th activity in sinking particles (here available only at $z = 2100$ m; Figure 4). Summing equations (1a–1c) gives a simple equation for total ^{230}Th,

$$0 = \lambda A_p - w\frac{\partial A_l}{\partial z}, \tag{10}$$

where it has been assumed that $T(\cdot) = 0$ and that the radioactive decay constant is negligible compared to other rate constants (a good approximation for ^{230}Th). Integrating this equation from depths z to 2100 m, assuming a vertically uniform w, and solving for w yield

$$w = (2100 - z)\lambda\frac{A_p}{A_l(2100 \text{ m}) - A_l(z)}. \tag{11}$$

With only one measurement of ^{230}Th in sinking particles (0.0019 dpm m^{-3} at $z = 2100$ m; Figure 4), w cannot be uniquely determined. If the ^{230}Th activity in particles vanishes at $z = 0$ m, as assumed in some models (e.g., *Bacon and Anderson* (1982)), the estimated value of w would be 75 m d^{-1}, which is half the actual value (150 m d^{-1}). Thus, the assumption of vanishing ^{230}Th$_l$ at $z = 0$ m leads to inaccurate recovery of w. A poor estimate of w was also obtained in our inversion where the posterior value of w is close to its prior value of 300 m d^{-1} (Figure 12). Note that the measurement of ^{230}Th in large particles at just one additional depth would allow w to be accurately estimated (if it is constant). For example, if the value ^{230}Th$_l$ = 0.001 dpm m^{-3} at $z = 110$ is known in addition to that at 2100 m, then application of (10) predicts a particle sinking speed of 150 m d^{-1} (keeping three significant digits), which is precisely the actual value.

Consider then the adsorption rate k_1 and the sum $k^*_{-1} = k_{-1} + \beta_{-1}$. Summing equations (1b–1c) leads to an equation for Th activity in all particles (small and large). Neglecting the sinking and radioactive decay of large particle activity compared to other terms in this equation,

$$\frac{k_1}{k^*_{-1} + \lambda} = \frac{A_s}{A_d}, \tag{12}$$

which is equation (13) in *Bacon and Anderson* (1982) (note that these authors did not explicitly consider particle remineralization, so k^*_{-1} is equivalent to k_{-1} in their equation). These authors used this equation to derive individual estimates of k_1 and k^*_{-1} from measurements of ^{230}Th and ^{234}Th activity on dissolved and particle fractions. Here the average value of A_s/A_d for the eight sampling depths (Figures 4 and 5) amounts to 0.16 for ^{230}Th and 0.037 for ^{234}Th, which lead to an estimate of 0.50 y^{-1} for k_1 and 3.2 y^{-1} for k^*_{-1}. These values are close to the actual ones (Table 2), in contrast to the results from our inversion (Figure 12). Given this result, the poor recovery of $k_{-1} + \beta_{-1}$ (Figure 12) may seem surprising. However, this result is obtained by assuming that the Th data and the approximate balance $k_1/(k^*_{-1} + \lambda) = A_s/A_d$ are perfectly accurate, whereas our inversion assumes data and model errors that should be more representative of oceanographic conditions. Should lower data and model errors be assumed, then the recovery of $k_{-1} + \beta_{-1}$ (and w) would be more successful and their posterior errors would be smaller, as illustrated in previous inversions (Figure 7; Figures 10 and 11).

4 DISCUSSION

In this section, the potential of Th and particle data to estimate rate constants of Th and particle cycling in the ocean is further explored. Emphasis is placed on (i) the ability to recover vertical variations in rate parameters, (ii) the contribution of ^{228}Th, ^{228}Ra, and particle data to parameter recovery, and (iii) the relative importance of ^{228,230}Th data in different size fractions. Three potential limitations of this study are then discussed. These are related to (i) the use of additional measurements to constrain the rate constants, (ii) the adequacy of the algorithm of total inversion as a general method to infer the rate parameters, and (iii) the interpretation of errors in the least-squares solution.

4.1 Vertical Variations in Rate Parameters

The inversions reported in section 3 are restricted to the case where the rate constants of Th and particle cycling that are to be estimated from Th and particle data are vertically uniform. As already stated it is plausible, however, that these 'constants' vary markedly in the deep sea. For example, significant depletion of ^{234}Th compared to secular equilibrium with its parent ^{238}U has been observed in benthic nepheloid layers (e.g., *Bacon and Rutgers van der Loeff* (1989); *Turnewitsch and Springer* (2001); *Rutgers van der Loeff et al.* (2002); *Inthorn et al.* (2006)). The relatively large $^{234}\text{Th}_s/^{234}\text{Th}_d$ ratio that is sometimes observed in these layers would result from a relatively large value of $k_1/(k_{-1}^* + \lambda)$, assuming equilibrium for sorption reactions (equation 12; *Bacon and Rutgers van der Loeff* (1989)).

The inverse method used in this study could also be applied to recover rate constants that vary along the water column. To illustrate this, an inversion is considered with two modifications compared to our reference inversion. First, Th adsorption onto small particles is assumed to be relatively slow except in a deep layer where it is faster. This case would represent a situation where particles suspended in deep water, such as MnO_2-rich particles in a benthic nepheloid layer (e.g., *Balistrieri and Murray* (1986); *Geibert and Usbeck* (2004)), have a high capacity for attaching Th onto their surfaces compared to particles in overlying water. Specifically, the following vertical profile is assumed for k_1,

$$k_1(z) = k_{1o}\left(1 + \alpha\phi\left(z\right)\right), \tag{13}$$

where $k_{1o} = 0.5$ y^{-1}, $\alpha = 0.2$, and $\phi(z) = \arctan((z - z_*)/l_*) + \pi/2$ with $z_* = 4000$ m and $l_* = 200$ m. This profile is characterized by quasi uniform values close to 0.5 y^{-1} above 3500 m, a sharp increase from 3500 m to 4500 m, and relatively uniform values below reaching a maximum of about 0.8 y^{-1} (solid line in Figure 14). Second, a source of small particles carrying the long-lived ^{230}Th is invoked near the bottom. The following source terms are added to the right-hand side of, respectively, the $^{230}\text{Th}_s$ equation (1b) and the small particle equation (3a):

$$ {}^{230}\dot{\mathrm{Th}}_s(z) = {}^{230}\dot{\mathrm{Th}}_{s,o}\,\phi(z) \qquad \text{and} \qquad \dot{P}_s(z) = \dot{P}_{s,o}\,\phi(z), \tag{14} $$

where ${}^{230}\dot{\mathrm{Th}}_{s,o} = 10^{-2}$ dpm m^{-3} y^{-1} and $\dot{P}_{s,o} = 10^{-5}$ kg m^{-3} y^{-1}. The sources described by (14) are relatively uniform above 3000 m, increase sharply from about 3500 to 4500 m, and are more uniform below (not shown). They would represent the effect of lateral transport of fine particles near the bottom or the effect of resuspension of fine particles from the seafloor, two processes that are thought to contribute to the formation and maintenance of benthic nepheloid layers in the ocean (e.g., *McCave* (1986)).

Profiles of ^{228,230,234}Th activity and particle concentration in the three size fractions are obtained by numerical solution of (1–3) with (i) k_1 varying according to (13) and (ii) the ${}^{230}\mathrm{Th}_s$ and small particle sources (14). The ^{228}Th profiles are qualitatively similar to those obtained with uniform k_1 (Figure 15). On the other hand, the ^{230}Th profiles are noticeably affected by the enhanced adsorption rate and the ${}^{230}\mathrm{Th}_s$ source in deep water (Figure 16). At depths greater than about 3500 m, the dissolved ^{230}Th activity shows lower values and the particle activities show larger values compared to those obtained with uniform k_1 and no ${}^{230}\mathrm{Th}_s$ source. The ^{234}Th activity in each size fraction is significantly influenced by enhanced k_1 in deep water (Figure 17): the dissolved activity shows lower values below 3500 m and the particle activities show higher values below 3500–4000 m relatively to the profiles computed with uniform k_1. Finally, the small and large particle concentrations show relative maxima below about 3500–4000 m, consistent with the presence of a particle source near the bottom (Figure 18).

An inversion is conducted in order to determine whether the vertical variations in the rate constant k_1 could be estimated from Th and particle data. The assumptions regarding the data and the model are the same as for the reference inversion: the data have a relative error of 5%, they are available at all depths, and model errors are very small ($p = 10^{-5}$). It is seen that the rates of Th adsorption estimated by inversion are all close and within two standard deviations of the actual values (Figure 14). The same result generally holds for the other rate constants (not shown). This result suggests that vertical variations of k_1

at a given oceanic location could be detected with high accuracy and precision, provided that data errors are reduced compared to their present values (Table 3), measurements are available with good vertical resolution, the $^{230}Th_s$ and small particle sources are known, and the model provides an accurate description of Th and particle cycling.

4.2 Contribution of ^{228}Th, ^{228}Ra, and Particle Data

Since this study is primarily motivated by GEOTRACES, it is probably worth clarifying further the sampling plans for GEOTRACES cruises. The sampling scheme considered here (section 2.1.1) corresponds only to one adopted at some of the deep stations occupied during the US GEOTRACES North Atlantic section. It does not apply to all stations of GEOTRACES sections but only to specific stations occupied during a specific cruise of this program. Furthermore, among the Th isotopes, only ^{230}Th is a key parameter to be measured on all GEOTRACES cruises. Thorium-228 would be measured rarely. The ^{228}Th activities are typically very low at mid-depth in the ocean, implying that a precise and accurate measurement of this nuclide would be challenging. A similar difficulty applies to its radioactive parent ^{228}Ra, also not a key parameter of GEOTRACES. Accordingly, the availability of ^{228}Th and ^{228}Ra data, which is assumed in this study, may be generally too optimistic. Thorium-234 will be determined on many but not all GEOTRACES cruises. Finally, the collection of particulate matter by in situ filtration (for Th analysis) is part of many GEOTRACES cruises but not all. Particle weights for small and large particles may not be available for many GEOTRACES expeditions.

Given these considerations, the contributions of ^{228}Th activity, ^{228}Ra activity, and particle concentration data to the estimation of rate constants of Th and particle cycling appear to deserve some discussion. Consider first the contribution of ^{228}Th data. In order to isolate this contribution, an inversion similar to our reference inversion (section 3.1) is performed but with the constraint provided by ^{228}Th dramatically reduced. Specifically, this new inversion assumes a relative error of 5% for all the data, their availability at all depths, and very small errors for the model equations ($p = 10^{-5}$) except for the ^{228}Th equations ($p = 1$). Compared to the reference inversion, the precision of the recovered rate parameters deteriorates noticeably except for k_1 (Figure 19). As the error factor for the ^{228}Th equations is increased from $p = 10^{-5}$ to $p = 1$, the relative precision ($\sigma_{\hat{x}}/\hat{x}$) of the posterior estimates changes from 0.06 to 0.07 for k_1, 0.20 to 0.33 for k_{-1}, 0.20 to 0.36 for w, 0.24 to 0.42 for β_{-1}, and 0.24 to 0.43 for β_2 and β_{-2} (all values are averages for the estimates at the six different depths displayed in Figure 19). Thus, the constraint provided by ^{228}Th data leads to a notable improvement in the relative precision of the rate constants, in particular of the rates of remineralization and (dis)aggregation.

Consider then the contribution of ^{228}Ra data. This contribution is illustrated from an inversion similar to the reference inversion except that (i) ^{228}Ra activity data are replaced by a constant value and (ii) the error for the dissolved ^{228}Th equation is increased. Assumptions (i)–(ii) would mimic those made for a location where an estimate of rate constants is desired but where ^{228}Ra activity data are not available. The ^{228}Ra activity at each depth is set equal to 2.4 dpm m^{-3}, which is twice the average value between 965 and 4900 m computed according to (2). Hence, the ^{228}Ra activities assumed in the inversion differ markedly from those used to generate the Th and particle data, an intentionally unfavourable situation. The error for the ^{228}Th$_d$ equation is set equal to the constant value of 2.4 dpm m^{-3} times the ^{228}Th radioactive decay constant. This assumption acknowledges that, given the use of a constant ^{228}Ra in the analysis, the error in the ^{228}Th$_d$ equation can be on the order of the radioactive source in this equation. It is seen that assumptions (i)–(ii) reduce to some extent the precision of most of the recovered rate constants compared to the reference inversion (Figure 20). The results are broadly comparable to those obtained for the case where the ^{228}Th constraint is reduced (Figure 19), although the relative precision of the estimated rate constants is better: when assumptions (i)–(ii) are made, the $\sigma_{\hat{x}}/\hat{x}$ ratio amounts to 0.07 for k_1, 0.26 for k_{-1}, 0.25 for w, 0.30 for β_{-1}, and 0.32 for β_2 and β_{-2} (all values are again averages for the estimates at the six different depths displayed in Figure 20).

Consider finally the contribution of particle concentration data. The contribution of these data to the estimation of the rate constants could in principle be isolated using the same approach as for ^{228}Th. However, our attempts to generate an inversion similar to our reference inversion but with the particle concentration constraints much reduced ($p = 1$ for the particle equations) have failed. We speculate that the lack of convergence of the objective function that occurs in this case is associated with the fact that estimates of all rate constants cannot be simultaneously obtained if the particle concentration constraints are much reduced or absent. Specifically, the rate constants of desorption and remineralization always appear as a sum in the Th equations (1a–1b), whereas in the particle equations (3a–3b) β_{-1} is present but k_{-1} is not. Accordingly, if only Th data are considered to infer the rate constants, the sum $k_{-1} + \beta_{-1}$ could be determined but not the individual values of k_{-1} and β_{-1}.

4.3 Importance of ^{228,230}Th Data in Different Size Fractions

Whereas the activity of the most abundant Th isotope (^{234}Th) would be measured with high accuracy, the activity of the other Th isotopes, in particular in the large particles, would not (Table 3). This state of affairs raises the question of whether ^{228}Th and ^{230}Th errors in all three size fractions are equally important for the estimation of the rate constants of Th and particle cycling.

To address this question, three inversions are performed, which differ from the reference inversion in the following respects. In a first inversion, the relative error in ^{228,230}Th data for the dissolved phase is raised to, respectively, 15% and 20% (Table 3). In a second inversion, the relative error in ^{228,230}Th data for small particles is fixed to the same values. Finally, in a third inversion, the relative error in ^{228,230}Th data for large particles is set equal to 20%. In each of these three inversions, the error for all the other data, the data availability, and the model errors are the same as those assumed in the reference inversion.

We find that, for each of these three inversions, the estimated rate constants differ generally from their actual values by less than two standard deviations (not shown). More relevant to the above question, the relative precision $\sigma_{\hat{x}}/\hat{x}$ varies by ≤ 0.07 for each rate constant between these inversions and the change in $\sigma_{\hat{x}}/\hat{x}$ is not systematic. That is, the presence of relatively high error for a given size fraction worsens the precision of some of the rate constants but improves the precision of others, compared to results obtained with relatively high error in another fraction. These results suggest that ^{228}Th and ^{230}Th should be measured with comparable (and high) accuracy in all size fractions if a precise estimate of all rate constants is sought.

4.4 Use of Additional Data

As shown by the present analysis, the extent to which measurements of a given property can constrain sportion and particle processes depends on the uncertainties in these measurements (data errors) as well as on our understanding of the behaviour of this property in the ocean (model errors). These processes will be completely unresolved if this property does not appear in the equations $\mathbf{f}(\mathbf{x}) = \mathbf{0}$ and if no correlation is introduced in $\mathbf{C}_o$ between this property and the other components included in $\mathbf{x}$. If this is not the case, then knowledge about sorptive reactions and particle dynamics should be increased compared to that obtained from, say, Th and particle data alone. The errors in the posterior estimates of the rate constants should be even more reduced compared to those in the prior estimates (e.g., Figure 1), the amount of reduction depending on the data errors ($\mathbf{C}_o$), the model errors ($\mathbf{C}_f$), and the sensitivity of the model equations to the components of $\mathbf{x}$ (*Tarantola and Valette*, 1982a).

Accordingly, this work is limited by the fact that not all types of measurement that may be available at stations occupied during modern oceanographic programs have been considered. Other properties may be available and provide additional information about rate constants of Th and particle cycling, such as the concentration of particulate organic carbon (POC), particulate organic nitrogen (PON), calcium carbonate ($CaCO_3$), biogenic silica (bSi), and another particle-reactive radio-isotope (protactinium-231). The concentration of Al, P, Ba, Pb, and transition elements (Ti, V, Mn, Fe, Co, Ni, Cu, Zn, and Cd) on different size fractions could also be measured and be useful to estimate cycling rates.

The motive for not including measurements of POC, PON, $CaCO_3$, bSi, and ^{231}Pa in our analysis is not only simplicity. It seems plausible that measurements of POC, PON,

$CaCO_3$, and bSi are the most likely to provide additional information about the cycling rates, not in the deep, but in the upper ocean (say, at $z < 1000$ m), where these properties tend to show large vertical gradients (e.g., *Lam et al.* (2011)). Besides, the kinetics of exchange with marine particles is even less constrained for Pa than for Th. Several studies have shown that Pa interacts in general less intensively with particles than Th, with exceptions such as MnO_2 precipitates and biogenic opal (e.g., *Anderson et al.* (1983); *Rutgers van der Loeff and Berger* (1993); *Walter et al.* (1997); *Chase et al.* (2002); *Moran et al.* (2002); *Geibert and Usbeck* (2004); *Scholten et al.* (2005); *Kretschmer et al.* (2011)). Consequently, the ability of ^{231}Pa activity data to significantly increase knowledge about processes such as particle coagulation and fragmentation over that already gained from Th and particle data does not seem to be obvious.

Still other types of data, however, might be used to further constrain sorption and particle processes at stations occupied along transoceanic sections. Whereas sediment traps are typically not deployed along such sections, sediment trap data from compilations (e.g., *Honjo et al.* (2008)) and local studies (e.g., *Roy-Barman et al.* (2005)) may provide useful constraints on the vertical flux of components such as POC, $CaCO_3$, bSi, and Th isotopes in some of the environments that are sampled along these sections. Particularly valuable would be data that would help better understand the relative importance of the trend and transport terms in the Th and particle equations. Better understanding of these terms would allow one to assume relatively small model errors and hence to better constrain the rate constants of Th and particle cycling. Vertical profiles of water density at adjacent stations might be used to estimate the vertical shear of the geostrophic velocity in the direction normal to the line joining the stations. Estimates of absolute velocity might then be obtained, provided that the velocity at some reference level is known or assumed. The product of absolute velocity times the horizontal gradient of Th isotope activity or particle concentration normal to the line could be derived at crossover stations, which would provide an estimate of the advection of Th or particles by the geostrophic flow along this direction. Moreover, measurements of core parameters such as temperature, salinity, dissolved oxygen, and dissolved nutrients could be consulted to identify whether features in the vertical profiles of Th isotope activities and particle concentrations could be associated with deep water masses of distinct origins. Short-lived isotopes such as ^{223}Ra (half life of 11.4 d) and ^{224}Ra (3.7 d) could be used to trace water transport from the margins over time scales of several days to weeks.

4.5 Appropriateness of Total Inversion

The method of total inversion has been applied in several studies aimed at interpreting Th and particle measurements on oceanic samples (e.g., *Murnane et al.* (1994); *Murnane* (1994); *Murnane et al.* (1996)). However, the appropriateness of this method to infer rate constants of trace metal and particle cycling has more recently been challenged (*Athias et al.*, 2000a; *Athias et al.*, 2000b). In particular, *Athias et al.* (2000b) argued that an approach based on a linearization around an a priori solution and on a gradient descent method is not adequate, given the complexity of the objective function and our poor a priori knowledge of the rate parameters. These authors presented results from twin experiments with a model of Al and particle cycling, which suggest that other minimization methods, such as genetic algorithms, are superior to the algorithm of total inversion for inferring the rate constants.

As acknowledged by *Tarantola and Valette* (1982a), the total inversion algorithm will only converge in problems where nonlinearity is not too strong. The source of nonlinearity for the present problem resides in the quadratic terms (products of variables in $\mathbf{x}$) that are present in the model equations $\mathbf{f}(\mathbf{x}) = \mathbf{0}$. Consequently, the total inversion algorithm should fail to converge in situations where Th and (or) particle data have relatively large errors *and* the model equations are imposed relatively strictly. For example, failure to converge is observed to occur in an inversion where the maximum relative error in the data is raised to 50% (so the relative errors take on the values in Table 3 for all data), the data are assumed to be available at all depths, and the model equations are assumed to be exact ($\mathbf{C}_f = \mathbf{0}$). On the other hand, this inversion does converge if even modest model errors are taken into consideration ($p = 0.1$). This example demonstrates that the performance of the total inversion algorithm depends on the specific data and model errors that are assumed by the investigator.

Accordingly, the total inversion algorithm may not be a generally applicable method to provide estimates of the cycling rates of trace metals and particles in the ocean. Alternative methods to provide such estimates, such as explored by *Athias et al.* (2000b), may be more universally applicable. On the other hand, the algorithm of total inversion has features that tend to make it attractive compared to other methods used to solve minimization problems, e.g., it can provide a formal estimate of the error in the solution and it does not require the prescription of parameters besides a criterion for convergence. The interpretation of posterior errors in the solution, however, is not always straightforward, as discussed below.

4.6 Interpretation of Error Estimates

The error estimates for the rate constants that are obtained by generalized least-squares are only approximate and do not all have a straightforward interpretation. First, the model equations $\mathbf{f}(\mathbf{x}) = \mathbf{0}$ are always imposed (in the mean square) in our inversions (if $\mathbf{f}(\mathbf{x}) = \mathbf{0}$ were not imposed, the problem would have the trivial solution $\mathbf{x} = \mathbf{x}_o$). This implies that nonlinearity is always present and that the error covariance matrix for the solution, which is obtained using the formula for the linear case, is always approximate (*Tarantola and Valette*, 1982a). On the other hand, all solutions reported in this paper are convergent, which suggests that nonlinearity is relatively weak and that the posterior variances of the rate 'constants', which these solutions provide, are useful estimates.

Second, the method of total inversion as applied here provides estimates of the standard deviation of the logarithm of the rate constants, not of their actual values. Although formula (8) allows posterior errors to be calculated, it assumes that the values obtained by inversion are the medians of normal distributions, which is not necessarily correct. Furthermore, the variance of a lognormal distribution determines not only the dispersion but also higher moments of the distribution such as skewness (*Aitchison and Brown*, 1957), in particular for variables with large spread around the mean (large variance). Accordingly, the large posterior errors for some of the rate constants that are estimated by inversion are relatively difficult to interpret. This is particularly the case for the rates of aggregation and disaggregation, which are among the parameters that are the most difficult to constrain from Th and particle data.

5 CONCLUSIONS

The rates at which particles are decomposed, settle, and (dis)aggregate in the ocean are of paramount importance from a geochemical viewpoint. However, they also are very difficult to estimate. A common approach to estimate these rates relies on measurements of particle-reactive elements, in particular Th radio-isotopes, on samples collected by bottles, in situ pumps, and sediment traps. Ongoing and future programs such as GEOTRACES are providing an unprecedented opportunity to estimate particle processes in a variety of oceanic settings. Whereas sediment traps are typically not deployed during large-scale sampling programs that are section-based, large volumes of water can now be collected over the entire water column during these programs. This sampling permits to document, at the same station, the vertical distribution of the activity of several Th isotopes and the vertical distribution of the concentration of particles, in different size fractions. The extent to which this unique set of observations could constrain the rates of Th and particle cycling in the ocean emerges as a question of preeminent interest.

Our study suggests that the data set gathered during modern sampling programs should improve very significantly our present understanding of the rates of Th and particle cycling in the deep sea. With current estimates of data uncertainties and plausible estimates of the uncertainty in Th and particle governing equations, the relative precision of rates of particle processes such as aggregation and disaggregation could be largely improved, sometimes by one order of magnitude, over that of prior estimates. On the other hand, estimates of cycling rates that are both precise and accurate would remain difficult to obtain, unless a significant effort is made to reduce the data uncertainties and the assumption of small model errors is justified. Accurate and precise estimates could be derived when (i) all the data have a relative error of less than 20%, (ii) vertical sampling is dense enough to resolve activity and concentration gradients, and (iii) model errors are negligible. In the favourable situation where (ii)–(iii) would hold, reducing the uncertainties in measurements of ^{228}Th and ^{230}Th activities and in particle concentrations from a maximum of 20% to a value of 5% would lead to a dramatic improvement in the estimates of the rate constants, in particular for Th desorption, particle sinking, and particle (dis)aggregation.

Overall, our study suggests that (i) analytical improvements should be prioritized on the measurement of ^{228}Th, ^{230}Th, and particle concentrations and (ii) Th and particle cycling rates should be estimated at locations where model assumptions are valid or where knowledge about temporal variability and transport processes is available. Accurate measurements of ^{228}Th and ^{230}Th in all size fractions would be needed for a precise estimation of all rate constants. Accurate measurements of ^{230}Th in large particles at only two depths should provide an important constraint on the particle sinking speed. Good candidates for the above locations include crossover stations away from ocean margins and where time series of oceanographic observations are available.

Acknowledgements.

The authors are grateful to Michiel Rutgers van der Loeff and to an anonymous reviewer for very useful comments that allowed us to significantly improve the manuscript. This study was stimulated by the GEOTRACES Data-Model Synergy Workshop on marine particles (Barcelona, November 2011). The authors would like to thank Robert Anderson for providing details about the uncertainties in ^{230}Th measurements on oceanic samples, for sharing figures illustrating unpublished results from an intercalibration effort undertaken as part of GEOTRACES, and for a discussion on preliminary results of this work. The provision by Matthew Charette of uncertainty estimates for ^{228}Th measurements on oceanic samples is also acknowledged.

References

Aitchison, J., and J. A. C. Brown. *The lognormal distribution (with special reference to its uses in economics).* Cambridge University Press, 1957. 176 pp.

Anderson, R. F., M. P. Bacon, and P. G. Brewer, Removal of ^{230}Th and ^{231}Pa at ocean margins, *Earth Planet. Sci. Lett.*, *66*, 73–90, 1983.

Athias, V., P. Mazzega, and C. Jeandel. Nonlinear inversions of a model of the oceanic dissolved-particulate exchanges, P. Kasibhatla, M. Heimann, P. Rayner, N. Mahowald, R. G. Prinn, and D. E. Hartley (Eds.), *Inverse methods in global biogeochemical cycles*, Volume 114 of *Geophysical Monograph*, pp. 205–222. Am. Geophys. Union, 2000a.

Athias, V., P. Mazzega, and C. Jeandel, Selecting a global optimization method to estimate the oceanic particle cycling rate constants, *J. Marine Res.*, *58*, 675–707, 2000b.

Bacon, M. P., and R. F. Anderson, Distribution of thorium isotopes between dissolved and particulate forms in the deep sea, *J. Geophys. Res.*, *87*, 2045–2056, 1982.

Bacon, M. P., C.-A. Huh, A. P. Fleer, and W. G. Deuser, Seasonality in the flux of natural radionuclides and plutonium in the deep Sargasso Sea, *Deep Sea Res.*, *32*, 273–286, 1985.

Bacon, M. P., C.-A. Huh, and R. M. Moore, Vertical profiles of some natural radionuclides over the Alpha Ridge, Arctic Ocean, *Earth Planet. Sci. Lett.*, *95*, 15–22, 1989.

Bacon, M. P., and M. M. Rutgers van der Loeff, Removal of thorium-234 by scavenging in the bottom nepheloid layer of the ocean, *Earth Planet. Sci. Lett.*, *92*, 157–164, 1989.

Balistrieri, L. S., and J. W. Murray, The surface chemistry of sediments from the Panama Basin: The influence of Mn oxides on metal adsorption, *Geochim. Cosmochim. Acta*, *50*, 2235–2243, 1986.

Berelson, W. M., Particle settling rates increase with depth in the ocean, *Deep Sea Res. II*, *49*, 237–251, 2002.

Boyd, P. W., and T. W. Trull, Understanding the export of biogenic particles in oceanic waters: Is there a concensus?, *Prog. Oceanogr.*, *72*, 276–312, 2007.

Brewer, P. G., Y. Nozaki, D. W. Spencer, and A. P. Fleer, Sediment trap experiments in the deep North Atlantic: Isotopic and elemental fluxes, *J. Marine Res.*, *38*, 703–728, 1980.

Broecker, W. S., and T.-H. Peng. *Tracers in the Sea.* Lamont-Doherty Geological Observatory, Palisades, NY: Eldigio Press, 1982.

Buesseler, K. O., C. Lamborg, P. Cai, R. Escoube, R. Johnson, S. Pike, P. Masque, D. McGillicuddy, and E. Verdeny, Particle fluxes associated with mesoscale eddies in the Sargasso Sea, *Deep Sea Res. II*, *55*, 1426–1444, 2008.

Burd, A. B., and G. A. Jackson, Particle aggregation, *Annu. Rev. Marine Sci.*, *1*, 65–90, 2009.

Chase, Z., R. F. Anderson, M. Q. Fleisher, and P. W. Kubik, The influence of particle composition and particle flux on the scavenging of Th, Pa and Be in the ocean, *Earth Planet. Sci. Lett.*, *204*, 215–229, 2002.

Chen, J. H., R. L. Edwards, and G. J. Wasserburg, ^{238}U, ^{234}U and ^{232}Th in seawater, *Earth Planet. Sci. Lett.*, *80*, 241–251, 1986.

Cheng, H., R. L. Edwards, J. Hoff, C. D. Gallup, D. A. Richards, and Y. Asmerom, The half-lives of uranium-234 and thorium-230, *Chem. Geol.*, *169*, 17–33, 2000.

Clegg, S. L., M. P. Bacon, and M. Whitfield, Application of a generalized scavenging model to thorium isotope and particle data at equatorial and high-latitude sites in the Pacific Ocean, *J. Geophys. Res.*, *96*, 20655–20670, 1991.

Clegg, S. L., and M. Whitfield, A generalized model for the scavenging of trace metals in the open ocean-I. Particle cycling, *Deep Sea Res.*, *37*, 809–832, 1990.

Clegg, S. L., and M. Whitfield, A generalized model for the scavenging of trace metals in the open ocean-II. Thorium scavenging, *Deep Sea Res.*, *38*, 91–120, 1991.

Cochran, J. K., K. O. Buesseler, M. P. Bacon, and H. D. Livingston, Thorium isotopes as indicators of particle dynamics in the upper ocean: Results from the JGOFS North Atlantic Bloom Experiment, *Deep Sea Res.*, *40*, 1569–1595, 1993.

Cochran, J. K., K. O. Buesseler, M. P. Bacon, H. W. Wang, D. J. Hirschberg, L. Ball, J. Andrews, G. Crossin, and A. P. Fleer, Short-lived thorium isotopes (^{234}Th, ^{228}Th) as indicators of POC export and particle cycling in the Ross Sea, Southern Ocean, *Deep Sea Res.*, *47*, 3451–3490, 2000.

Cochran, J. K., H. D. Livingston, D. J. Hirschberg, and L. D. Surprenant, Natural and anthropogenic radionuclide distributions in the northwestern Atlantic Ocean, *Earth Planet. Sci. Lett.*, *84*, 135–152, 1987.

Fischer, G., and G. Karakaş, Sinking rates and ballast composition of particles in the Atlantic Ocean: Implications for the organic carbon fluxes to the deep ocean, *Biogeosciences*, *6*, 85–102, 2009.

Geibert, W., and R. Usbeck, Adsorption of thorium and protactinium onto different particle types: Experimental findings, *Geochim. Cosmochim. Acta*, *68*, 1489–1501, 2004.

GEOTRACES, 2006. An international study of the marine biogeochemical cycles of trace elements and their isotopes. Science plan, Scientific Committee on Oceanic Research, International Council for Science.

Hirose, K., T. Saito, S. H. Lee, and J. Gastaud, Vertical distributions of the strong organic ligand in the twilight zone of Southern Hemisphere Ocean particulate matter, *Prog. Oceanogr.*, *89*, 108–119, 2011.

Honjo, S., S. J. Manganini, R. A. Krishfield, and R. François, Particulate organic carbon fluxes to the ocean interior and factors controlling the biological pump: A synthesis of global sediment trap programs since 1983, *Prog. Oceanogr.*, *76*, 217–285, 2008.

Inthorn, M., M. Rutgers van der Loeff, and M. Zabel, A study of particle exchange at the sediment-water interface in the Bengulea upwelling area based on ^{234}Th/^{238}U disequilibrium, *Deep Sea Res. I*, *53*, 1742–1761, 2006.

Key, R. M., J. L. Sarmiento, and W. S. Moore, 1992. Transient Tracers in the Ocean North Atlantic Study, Final Data Report for ^{228}Ra and ^{226}Ra. Technical report, 92-2, Ocean Tracer Lab. Princeton University, Princeton, N. J.

Kretschmer, S., W. Geibert, M. M. Rutgers van der Loeff, C. Schnabel, S. Xu, and G. Mollenhauer, Fractionation of ^{230}Th, ^{231}Pa, and ^{10}Be induced by particle size and composition within an opal-rich sediment of the Atlantic Southern Ocean, *Geochim. Cosmochim. Acta*, *75*, 6971–6987, 2011.

Lam, P. J., S. C. Doney, and J. K. B. Bishop, The dynamic ocean biological pump: Insights from a global compilation of particulate organic carbon, $CaCO_3$, and opal concentration profiles from the mesopelagic, *Global Biogeochem. Cycles*, *25*, GB3009, doi:10.1029/2010GB003868, 2011.

Lepore, K., and S. B. Moran, Seasonal changes in thorium scavenging and particle aggregation in the western Arctic Ocean, *Deep Sea Res.*, *54*, 919–938, 2007.

Liebelt, P. B. *An introduction to optimal estimation.* Addison-Wesley, Reading, MA, 1967. 273 pp.

Lohrenz, S. E., G. A. Knauer, V. L. Asper, M. Tuel, A. F. Michaels, and A. H. Knap, Seasonal variability in primary production and particle flux in the northwestern Sargasso Sea: U.S. JGOFS Bermuda Atlantic Time-series Study, *Deep Sea Res.*, *39*, 1373–1391, 1992.

Marchal, O., R. François, and J. Scholten, Contribution of ^{230}Th measurements to the estimation of the abyssal circulation, *Deep Sea Res.*, *54*, 557–585, 2007.

McCave, I. N., Local and global aspects of the bottom nepheloid layers in the world ocean, *Neth. J. Sea Res.*, *20*, 167–181, 1986.

McDonnell, A., and K. Buesseler, Variability in the average sinking velocity of marine particles, *Limnol. Oceanogr.*, *55*, 2085–2096, 2010.

Moran, S. B., M. A. Charette, J. A. Hoff, R. L. Edwards, and W. M. Landing, Distribution of ^{230}Th in the Labrador Sea and its relation to ventilation, *Earth Planet. Sci. Lett.*, *150*, 151–160, 1997.

Moran, S. B., C.-C. Shen, H. N. Edmonds, S. E. Weinstein, J. N. Smith, and R. L. Edwards, Dissolved and particulate ^{231}Pa and ^{230}Th in the Atlantic Ocean: Constraints on intermediate/deep water age, boundary scavenging, and ^{231}Pa/^{230}T fractionation, *Earth Planet. Sci. Lett.*, *203*, 999–1014, 2002.

Murnane, R. J., Determination of thorium and particulate matter cycling parameters at station P: A reanalysis and comparison of least squares techniques, *J. Geophys. Res.*, *99*, 3393–3405, 1994.

Murnane, R. J., J. K. Cochran, K. O. Buesseler, and M. P. Bacon, Least-squares estimates of thorium, particle, and nutrient cycling rate constants from the JGOFS North Atlantic Bloom Experiment, *Deep Sea Res.*, *43*, 239–258, 1996.

Murnane, R. J., J. K. Cochran, and J. L. Sarmiento, Estimates of particle- and thorium-cycling rates in the northwest Atlantic Ocean, *J. Geophys. Res.*, *99*, 3373–3392, 1994.

Murnane, R. J., J. L. Sarmiento, and M. P. Bacon, Thorium isotopes, particle cycling models, and inverse calculations of model rate constants, *J. Geophys. Res.*, *95*, 16,195–16,206, 1990.

Nozaki, Y., Y. Horibe, and H. Tsubota, The water column distributions of thorium isotopes in the western North Pacific, *Earth Planet. Sci. Lett.*, *54*, 203–216, 1981.

Nozaki, Y., H.-S. Yang, and M. Yamada, Scavenging of thorium in the ocean, *J. Geophys. Res.*, *92*, 772–778, 1987.

Owens, S. A., K. O. Buesseler, and K. W. W. Sims, Re-evaluating the ^{238}U–salinity relationship in seawater: Implications for the ^{238}U–^{234}Th disequilibrium method, *Mar. Chem.*, *127*, 31–39, 2011.

Robinson, L. F., N. S. Belshaw, and G. M. Henderson, U and Th concentrations and isotope ratios in modern carbonates and waters from the Bahamas Bank, *Geochim. Cosmochim. Acta*, *68*, 1777–1789, 2004.

Roy-Barman, M., J. H. Chen, and G. J. Wasserburg, ^{230}Th–^{232}Th systematics in the central Pacific Ocean: The sources and fates of thorium, *Earth Planet. Sci. Lett.*, *139*, 351–363, 1996.

Roy-Barman, M., C. Jeandel, M. Souhaut, M. Rutgers van der Loeff, I. Voege, N. LeBlond, and R. Freydier, The influence of particle composition on thorium scavenging in the NE Atlantic ocean (POMME experiment), *Earth Planet. Sci. Lett.*, *240*, 681–693, 2005.

Rutgers van der Loeff, M. M., and G. W. Berger, Scavenging of ^{230}Th and ^{231}Pa near the Antarctic Polar Front in the South Atlantic, *Deep Sea Res. I*, *40*, 339–357, 1993.

Rutgers van der Loeff, M. M., R. Meyer, B. Rudels, and E. Rachor, Resuspension and particle transport in the benthic nepheloid layer and near Fram Strait in relation to faunal abundances and ^{234}Th depletion, *Deep Sea Res. I*, *49*, 1941–1958, 2002.

Scholten, J. C., J. Fietzke, A. Mangini, P. Stoffers, T. Rixen, B. Gaye-Haake, T. Blanz, V. Ramaswamy, F. Sirocko, H. Schulz, and V. Ittekot, Radionuclide fluxes in the Arabian Sea: The role of particle composition, *Earth Planet. Sci. Lett.*, *230*, 319–337, 2005.

Sweeney, E. N., D. J. McGillicuddy, and K. O. Buesseler, Biogeochemical impacts due to mesoscale eddy activity in the Sargasso Sea as measured at the Bermuda Atlantic Time-series Study (BATS), *Deep Sea Res. II*, *50*, 3017–3039, 2003.

Tarantola, A., and B. Valette, Generalized nonlinear inverse problem solved using the least squares criterion, *Rev. Geophys. Space Phys.*, *20*, 219–232, 1982a.

Tarantola, A., and B. Valette, Inverse problem = quest for information, *J. Geophys.*, *50*, 159–170, 1982b.

Turnewitsch, R., and B. M. Springer, Do bottom mixed layers influence ^{234}Th dynamics in the abyssal near-bottom water column?, *Deep Sea Res.*, *48*, 1279–1307, 2001.

Venchiarutti, C., C. Jeandel, and M. Roy-Barman, Particle dynamics study in the wake of Kerguelen Island using thorium isotopes, *Deep Sea Res. I*, *55*, 1343–1363, 2008.

Venchiarutti, C., M. Rutgers van der Loeff, and I. Stimac, Scavenging of ^{231}Pa and thorium isotopes based on dissolved and size-fractionated particulate distributions at Drake Passage (ANTXXIV-3), *Deep Sea Res. II*, *58*, 2767–2784, 2011.

Vogler, S., J. Scholten, M. Rutgers van der Loeff, and A. Mangini, ^{230}Th in the eastern North Atlantic: the importance of water mass ventilation in the balance of ^{230}Th, *Earth Planet. Sci. Lett.*, *156*, 61–74, 1998.

Walter, H. J., M. M. Rutgers van der Loeff, and H. Hoeltzen, Enhanced scavenging of ^{231}Pa relative to ^{230}Th in the South Atlantic south of the Polar Front: Implications for the use of the ^{231}Pa/^{230}Th ratio as a paleoproductivity proxy, *Earth Planet. Sci. Lett.*, *149*, 85–100, 1997.

Table 1. ^{228,230,234}Th half-lifes and parent activities

	Half-life^a	Parent	Parent activity^b
^{228}Th	1.91 yr	^{228}Ra	variable
^{230}Th	75.69×10^3 yr	^{234}U	2.7×10^3 dpm m^{-3}
^{234}Th	24.1 d	^{238}U	2.4×10^3 dpm m^{-3}

^{a} The ^{228}Th and ^{234}Th half-lifes are from *Broecker and Peng* (1982). The ^{230}Th half-life is from *Cheng et al.* (2000)

^{b} The ^{238}U activity is based on an empirical relationship with salinity (*Owens et al.*, 2011) assuming a salinity of 35. The ^{234}U activity is derived from the resulting ^{238}U activity value and a seawater ^{234}U/^{238}U ratio of 1.14 (*Chen et al.*, 1986; *Robinson et al.*, 2004).

Table 2. Rate constants of thorium and particle cycling

Symbol	Definition	Model Value^a	Prior Estimate ^{a}	Relative Error^b
k_1	Adsorption rate	0.5	5	1
k_{-1}	Desorption rate	2	5	1
w	Sinking rate	150	300	0.5
β_{-1}	Remineralization rate	1	10	5
β_2	Aggregation rate	3	10	10
β_{-2}	Disaggregation rate	150	500	10

^{a} All values are in y^{-1}, except for w that is in m d^{-1}

^{b} The relative error pertains to the prior estimate

Table 3. Relative errors in measurement of ^{228,230,234}Th and particle concentration†

	Definition	Relative error
$^{228}Th_d$	^{228}Th activity in dissolved phase	±0.15
$^{228}Th_s$	^{228}Th activity in small particles	±0.15
$^{228}Th_l$	^{228}Th activity in large particles	±0.50
$^{230}Th_d$	^{230}Th activity in dissolved phase	±0.20
$^{230}Th_s$	^{230}Th activity in small particles	±0.20
$^{230}Th_l$	^{230}Th activity in large particles	±0.50
$^{234}Th_d$	^{234}Th activity in dissolved phase	±0.05
$^{234}Th_s$	^{234}Th activity in small particles	±0.05
$^{234}Th_l$	^{234}Th activity in large particles	±0.05
P_s	Concentration of small particles	±0.20
P_l	Concentration of large particles	±0.20

†Note our reference inversion assumes a relative error of 5% for all measurements

Figure 1: Published estimates of rate constants of (1) thorium adsorption (k_1) and desorption (k_{-1}) and (2) particle remineralization (β_{-1}), aggregation (β_2), and disaggregation (β_{-2}). The numbers along the lower horizontal axis are 0 for *Nozaki et al.* (1987), 1 for *Bacon et al.* (1989), 2 for *Bacon and Anderson* (1982), 3 for *Nozaki et al.* (1981), 4 for *Clegg et al.* (1991), 5 for *Clegg and Whitfield* (1991), 6 for *Murnane et al.* (1990), 7 for *Murnane et al.* (1994), 8 for *Murnane* (1994), and 9 for *Murnane et al.* (1996). The plotted values are those compiled by *Murnane et al.* (1994) and *Murnane* (1994) (cf. Table 1 of these two papers) as well as those obtained in these two studies and by *Murnane et al.* (1996). They include (i) point estimates with errors (solid circles with vertical bars), (ii) ranges, and (iii) point estimates without error (solid circles alone). The error bars in contact with the lower horizontal axis reach negative values and cannot be shown on a logarithmic scale. Some of the intervals (ranges) reported in the compilations or original publications are open, implying a larger error than it appears on the figure. Note that not all published estimates are shown to avoid congestion of the figure.

Figure 2: Schematic diagram of the cycling of trace metals (top) and particles (bottom) in the ocean aphotic zone. Metal activity is partitioned between the dissolved phase (A_d), the small particles (A_s) and the large particles (A_l). Particle concentration is partitioned between the small particles (P_s) and the large particles (P_l). The processes affecting metal activity and particle concentration in these different forms are the production by the radioactive parent (A_p), the radioactive decay (at a specific rate λ), the adsorption onto small particles (k_1), the desorption from small particles (k_{-1}), the remineralization of small particles (β_{-1}), the aggregation of small particles (β_2), the disaggregation of large particles (β_{-2}), and the sinking of large particles (with velocity w).

Figure 3: Vertical profiles of ^{228}Th activity in the dissolved phase (upper horizontal axis), the small particles (middle axis), and the large particles (lower axis). The ^{228}Th activities that are obtained from the analytical (numerical) solution of the model are shown by solid (dashed) lines. The two lines are barely distinguishable. The ^{228}Th activities at sampling depths, which are used to produce the idealized data for the inversions, are shown by circles: open circles for the dissolved phase, small solid circles for the small

particles, and large solid circles for the large particles. The horizontal bars show the errors in these activities. These activities are shown only at some of the pumping depths at GEOTRACES NA deep stations.

Figure 4: Same as Figure 3 but for ^{230}Th.

Figure 5: Same as Figure 3 but for ^{234}Th.

Figure 6: Same as Figure 3 but for the concentration of particles. The concentration of small (large) particles is shown by small (large) circles.

Figure 7: Rate constants of Th and particle cycling estimated with varying data errors. The vertical solid lines indicate the values used to generate Th and particle data. The vertical dashed lines indicate the prior estimates assumed in the inversions. The solid circles with horizontal bars show the means with their errors estimated in an inversion where data have a relative error of 5% (reference inversion). The open circles (crosses) with horizontal bars show the means (medians) with their errors estimated in an inversion where data have a relative error of ≤ 20 %. In both inversions, data are available at all depths and model errors are assumed to be very small ($p = 10^{-5}$). The rate constants estimated by inversion are shown at six of the pumping depths at GEOTRACES NA deep stations.

Figure 8: Effect of maximum data error on the accuracy of the rate constants of Th and particle cycling estimated by inversion. The accuracy is measured by the difference between the estimated value and the actual value, divided by the actual value.

Figure 9: Effect of maximum data error on the precision of the rate constants of Th and particle cycling estimated by inversion. The precision is measured by the ratio between the standard deviation of the estimated value and the estimated value.

Figure 10: Rate constants of Th and particle cycling estimated with varying model errors. The vertical solid lines indicate the values used to generate Th and particle data. The vertical dashed lines indicate the prior estimates assumed in the inversions. The solid circles with horizontal bars show the means with their errors estimated in an inversion

where $p = 0.1$. The open circles with horizontal bars (crosses) show the means (medians) with their errors estimated in an inversion where $p = 1$. In both inversions, the data have no error and are available at all depths. The rate constants estimated by inversion are shown at six of the pumping depths at GEOTRACES NA deep stations.

Figure 11: Rate constants of Th and particle cycling estimated with varying sampling schemes. The vertical solid lines indicate the values used to generate Th and particle data. The vertical dashed lines indicate the prior estimates assumed in the inversions. The solid circles with horizontal bars show the means with their errors estimated in an inversion where data are available at all depths. The open circles (crosses) with horizontal bars show the means (medians) with their errors estimated in an inversion where data are interpolated or extrapolated. In both inversions, the data have no error (except in the second inversion where extrapolated values have a relative error of 1) and the factor for model errors $p = 0.01$. The rate constants estimated by inversion are shown at six of the pumping depths at GEOTRACES NA deep stations.

Figure 12: Rate constants of Th and particle cycling estimated in the presence of data errors, model errors, and limited sampling. The vertical solid lines indicate the values used to generate Th and particle data. The vertical (horizontal) dashed lines indicate the prior estimates (their errors) assumed in the inversions. The open circles (crosses) with horizontal bars show the means (medians) and their errors estimated in an inversion where (i) the errors and depths of the measurements would be those at GEOTRACES NA deep stations and (ii) the factor for model errors $p = 1$. The rate constants estimated by inversion are shown at six of the pumping depths at these stations.

Figure 13: Cumulative distribution function (CDF) of the relative precision of the rate constants of Th and particle cycling, which are estimated in the presence of data errors, model errors, and limited sampling. The relative precision is the standard deviation of the rate constant divided by the value of the rate constant. The dashed (solid) line is the CDF for the prior (posterior) estimates. Also shown is the CDF of the difference between the estimated and actual value, divided by the standard deviation of the estimated value (dotted line). Note that the CDFs for the posterior estimates are based on values at all

depths of the model grid.

Figure 14: Recovery of vertical variations in the rate constant of Th adsorption. The solid line indicates values used to generate Th and particle data. The solid circles with horizontal bars show the means with their errors estimated in an inversion where the data have a relative error of 5%, they are available at all depths, and model errors are very small ($p = 10^{-5}$). Note that the values estimated by inversion are shown only at some of the pumping depths at GEOTRACES NA deep stations.

Figure 15: Vertical profiles of ^{228}Th activity in the dissolved phase (upper horizontal axis), the small particles (middle axis), and the large particles (lower axis). The ^{228}Th activities that are obtained by numerical solution with uniform (variable) rate of Th adsorption are shown by dashed (solid) lines (left most lines for large particles, middle lines for the dissolved phase, and right most lines for small particles).

Figure 16: Same as Figure 15 but for ^{230}Th (left most lines for large particles, middle lines for small particles, and right most lines for the dissolved phase).

Figure 17: Same as Figure 15 but for ^{234}Th (left most lines for large particles, middle lines for small particles, and right most lines for the dissolved phase).

Figure 18: Same as Figure 15 but for the concentration of particles (left lines for large particles and right lines for small particles).

Figure 19: Rate constants of Th and particle cycling estimated with varying errors in the ^{228}Th equations. The vertical solid lines indicate the values used to generate Th and particle data. The vertical dashed lines indicate the prior estimates of the rate constants assumed in the inversions. The solid circles with horizontal bars show the means with their errors estimated in the reference inversion. The open circles (crosses) with horizontal bars show the means (medians) with their errors estimated in an inversion with a relatively large error for the ^{228}Th equations ($p = 1$). In both inversions, the data have a relative error of 5% and are available at all depths. The rate constants estimated by inversion are shown at six of the pumping depths at GEOTRACES NA deep stations.

Figure 20: Rate constants of Th and particle cycling estimated with or without local ^{228}Ra data. The vertical solid lines indicate the values used to generate Th and particle data. The vertical dashed lines indicate the prior estimates assumed in the inversions. The solid circles with horizontal bars show the means with their errors estimated in the reference inversion. The open circles (crosses) with horizontal bars show the means (medians) with their errors estimated in an inversion where (i) ^{228}Ra activity is fixed to 2.4 dpm m^{-3} at all depths and (ii) the error in the ^{228}Th$_d$ equation is set equal to this value times the ^{228}Th radioactive decay constant. The rate constants estimated by inversion are shown at six of the pumping depths at GEOTRACES NA deep stations.

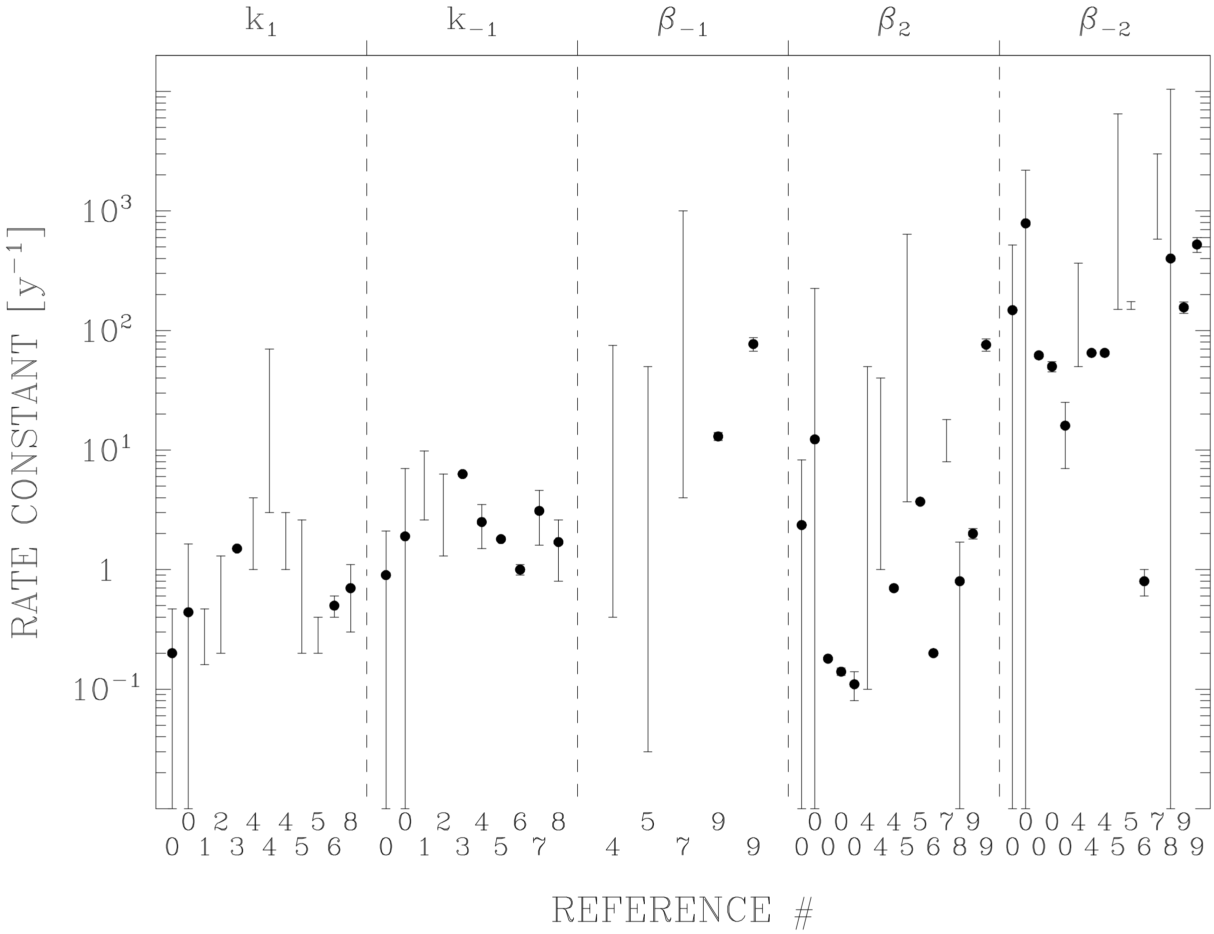

Figure 1: Published estimates of rate constants of (1) thorium adsorption (k_1) and desorption (k_{-1}) and (2) particle remineralization (β_{-1}), aggregation (β_2), and disaggregation (β_{-2}). The numbers along the lower horizontal axis are 0 for *Nozaki et al.* (1987), 1 for *Bacon et al.* (1989), 2 for *Bacon and Anderson* (1982), 3 for *Nozaki et al.* (1981), 4 for *Clegg et al.* (1991), 5 for *Clegg and Whitfield* (1991), 6 for *Murnane et al.* (1990), 7 for *Murnane et al.* (1994), 8 for *Murnane* (1994), and 9 for *Murnane et al.* (1996). The plotted values are those compiled by *Murnane et al.* (1994) and *Murnane* (1994) (cf. Table 1 of these two papers) as well as those obtained in these two studies and by *Murnane et al.* (1996). They include (i) point estimates with errors (solid circles with vertical bars), (ii) ranges, and (iii) point estimates without error (solid circles alone). The error bars in contact with the lower horizontal axis reach negative values and cannot be shown on a logarithmic scale. Some of the intervals (ranges) reported in the compilations or original publications are open, implying a larger error than it appears on the figure. Note that not all published estimates are shown to avoid congestion of the figure.

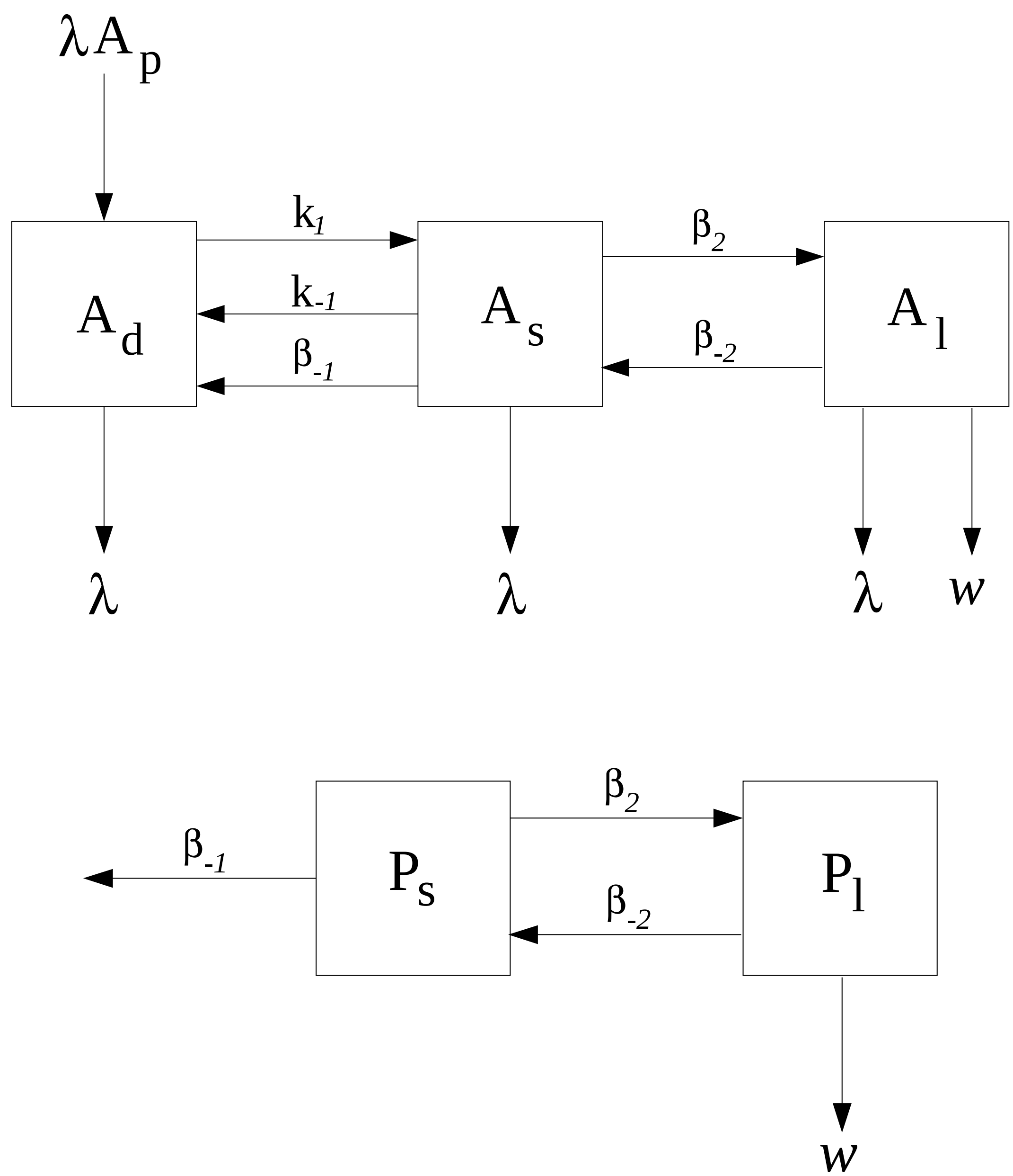

Figure 2: Schematic diagram of the cycling of trace metals (top) and particles (bottom) in the ocean aphotic zone. Metal activity is partitioned between the dissolved phase (A_d), the small particles (A_s) and the large particles (A_l). Particle concentration is partitioned between the small particles (P_s) and the large particles (P_l). The processes affecting metal activity and particle concentration in these different forms are the production by the radioactive parent (A_p), the radioactive decay (at a specific rate λ), the adsorption onto small particles (k_1), the desorption from small particles (k_{-1}), the remineralization of small particles (β_{-1}), the aggregation of small particles (β_2), the disaggregation of large particles (β_{-2}), and the sinking of large particles (with velocity w).

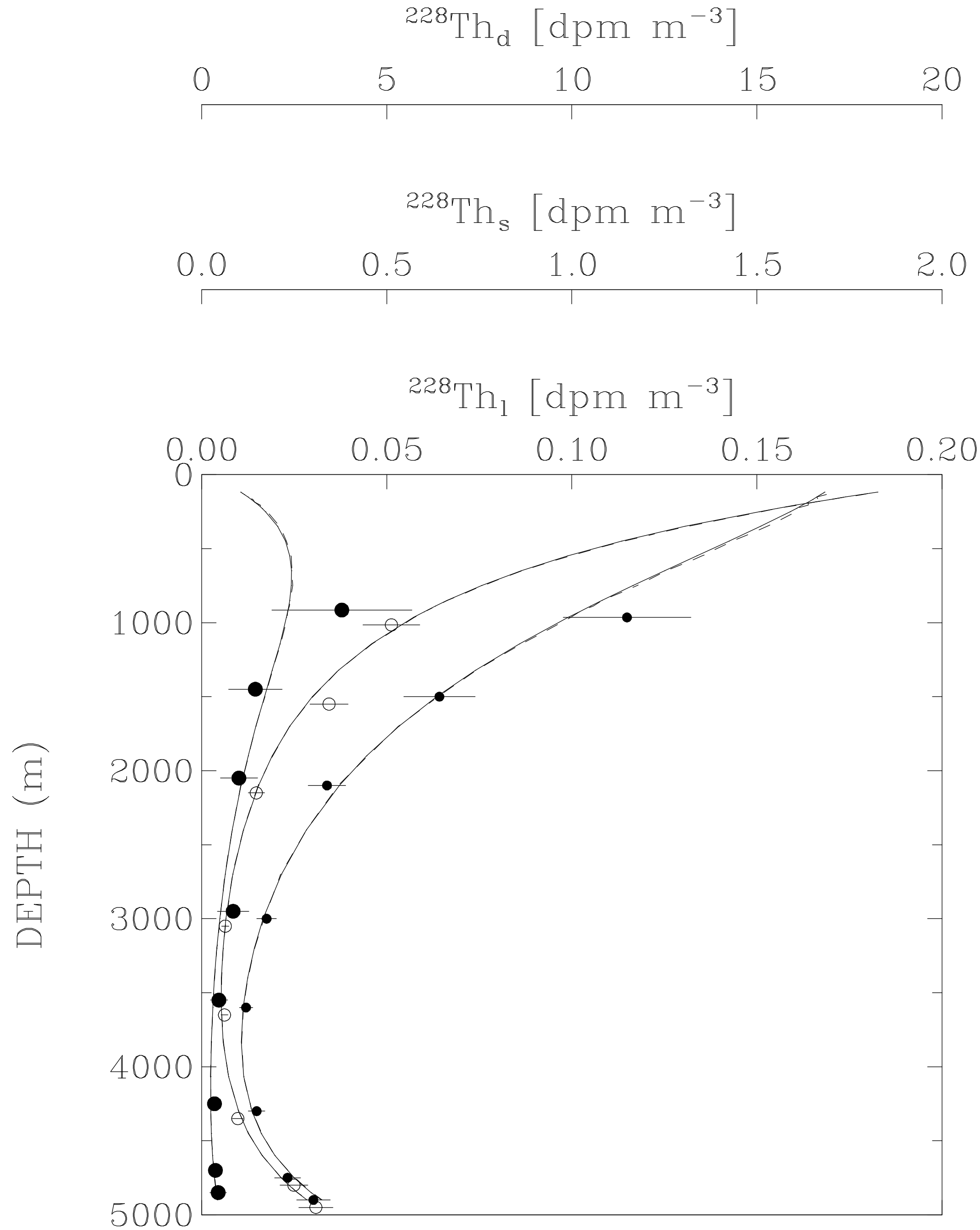

Figure 3: Vertical profiles of ^{228}Th activity in the dissolved phase (upper horizontal axis), the small particles (middle axis), and the large particles (lower axis). The ^{228}Th activities that are obtained from the analytical (numerical) solution of the model are shown by solid (dashed) lines. The two lines are barely distinguishable. The ^{228}Th activities at sampling depths, which are used to produce the idealized data for the inversions, are shown by circles: open circles for the dissolved phase, small solid circles for the small particles, and large solid circles for the large particles. The horizontal bars show the errors in these activities. These activities are shown only at some of the pumping depths at GEOTRACES NA deep stations.

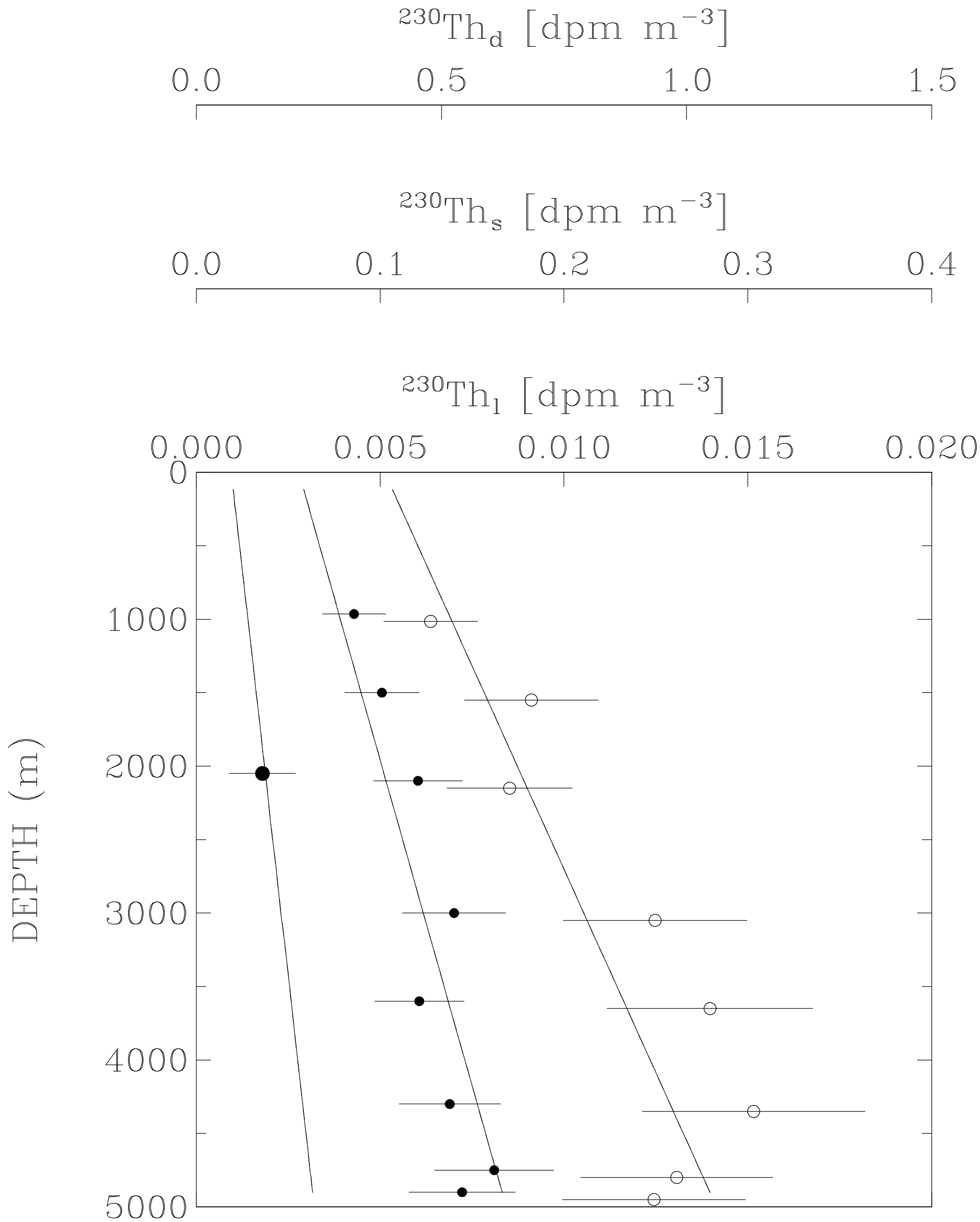

Figure 4: Same as Figure 3 but for ^{230}Th.

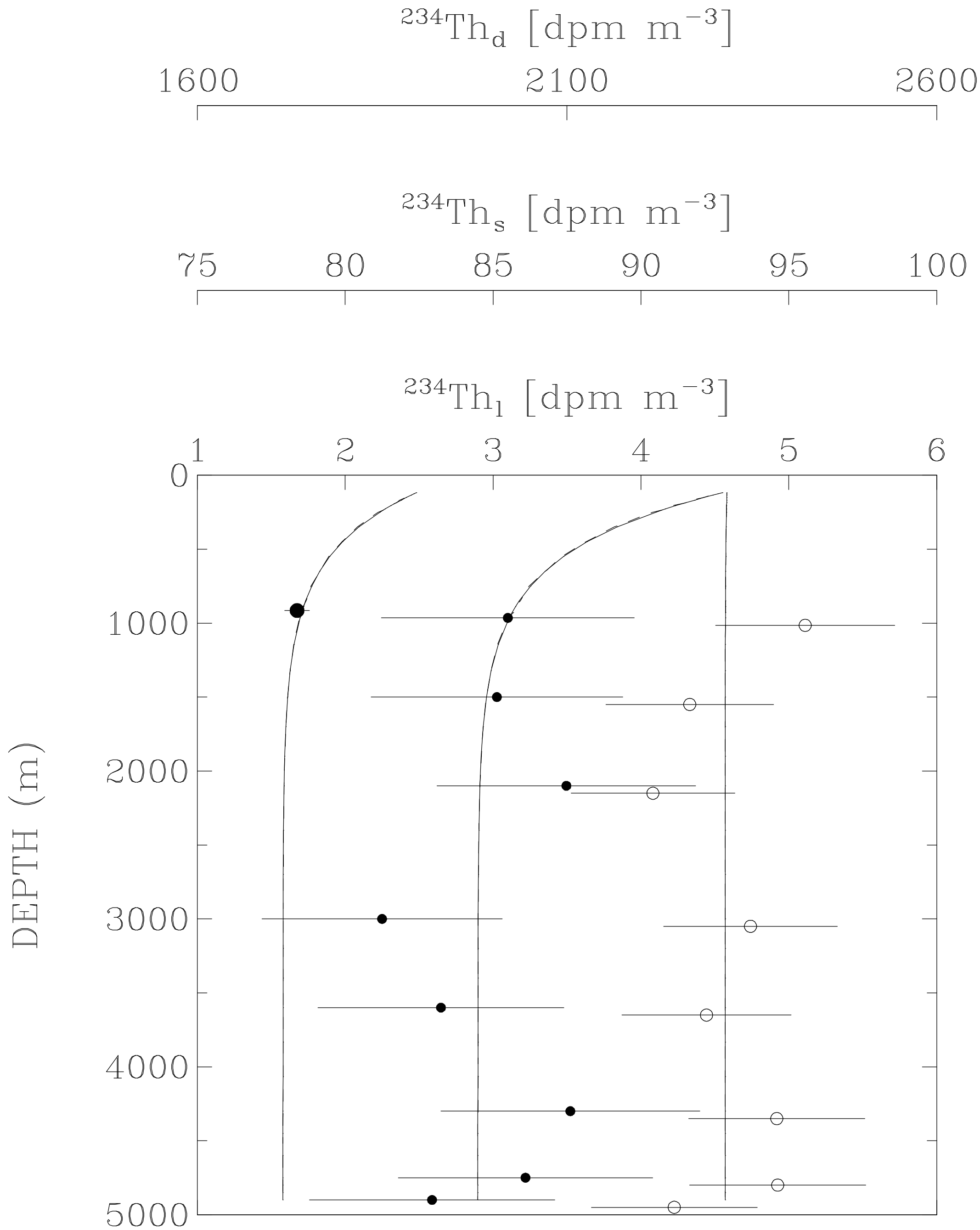

Figure 5: Same as Figure 3 but for ^{234}Th.

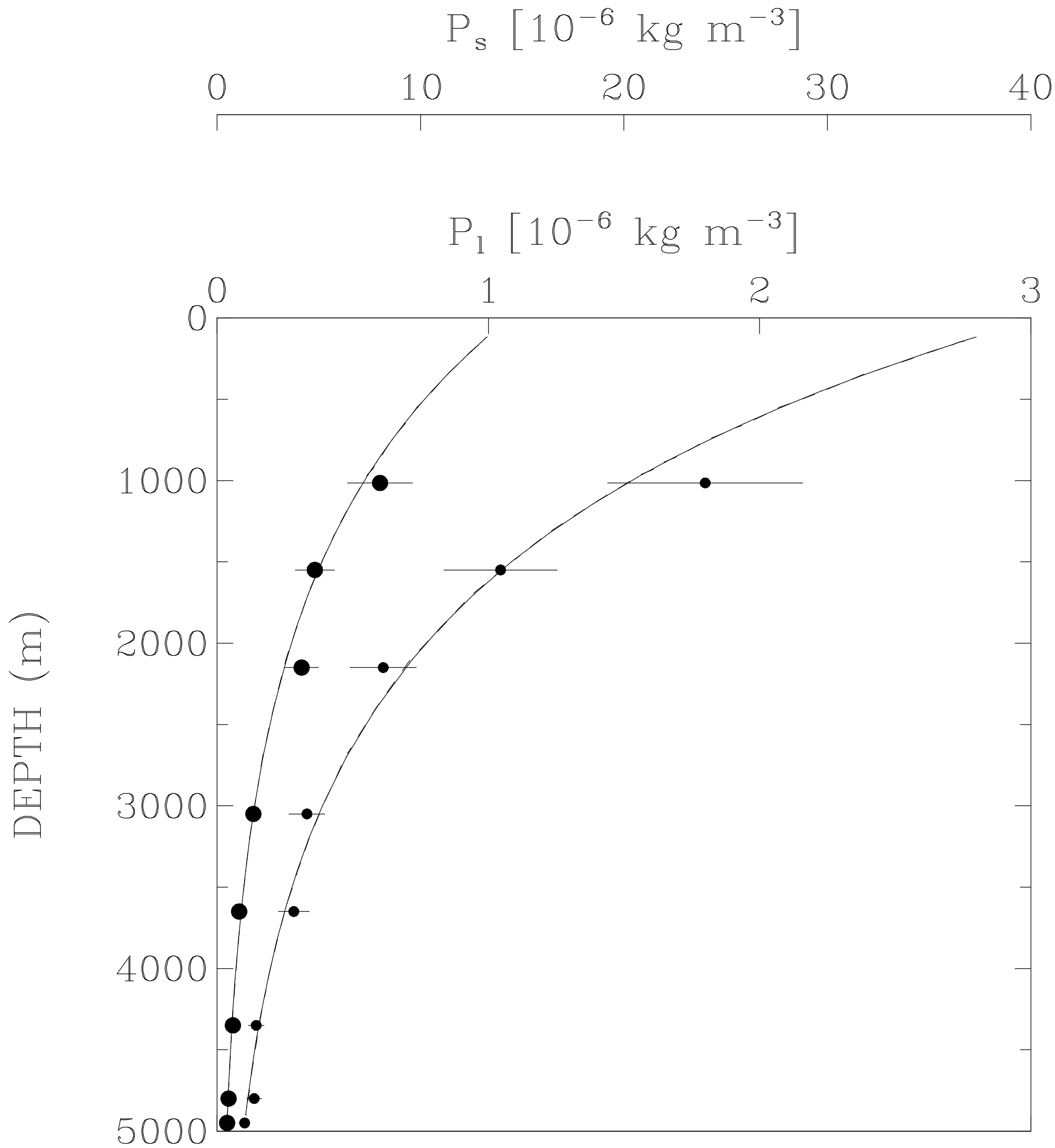

Figure 6: Same as Figure 3 but for the concentration of particles. The concentration of small (large) particles is shown by small (large) circles.

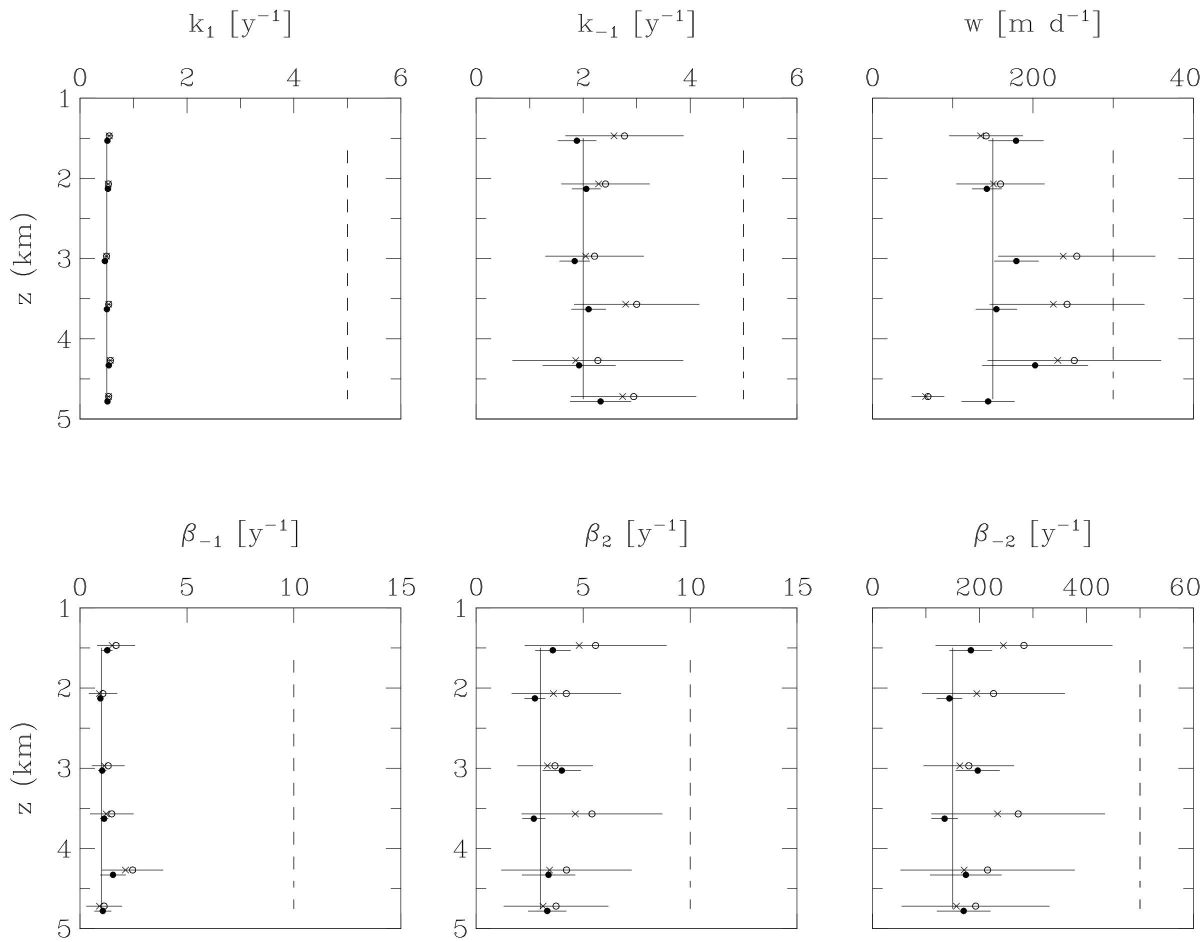

Figure 7: Rate constants of Th and particle cycling estimated with varying data errors. The vertical solid lines indicate the values used to generate Th and particle data. The vertical dashed lines indicate the prior estimates assumed in the inversions. The solid circles with horizontal bars show the means with their errors estimated in an inversion where data have a relative error of 5% (reference inversion). The open circles (crosses) with horizontal bars show the means (medians) with their errors estimated in an inversion where data have a relative error of ≤ 20 %. In both inversions, data are available at all depths and model errors are assumed to be very small ($p = 10^{-5}$). The rate constants estimated by inversion are shown at six of the pumping depths at GEOTRACES NA deep stations.

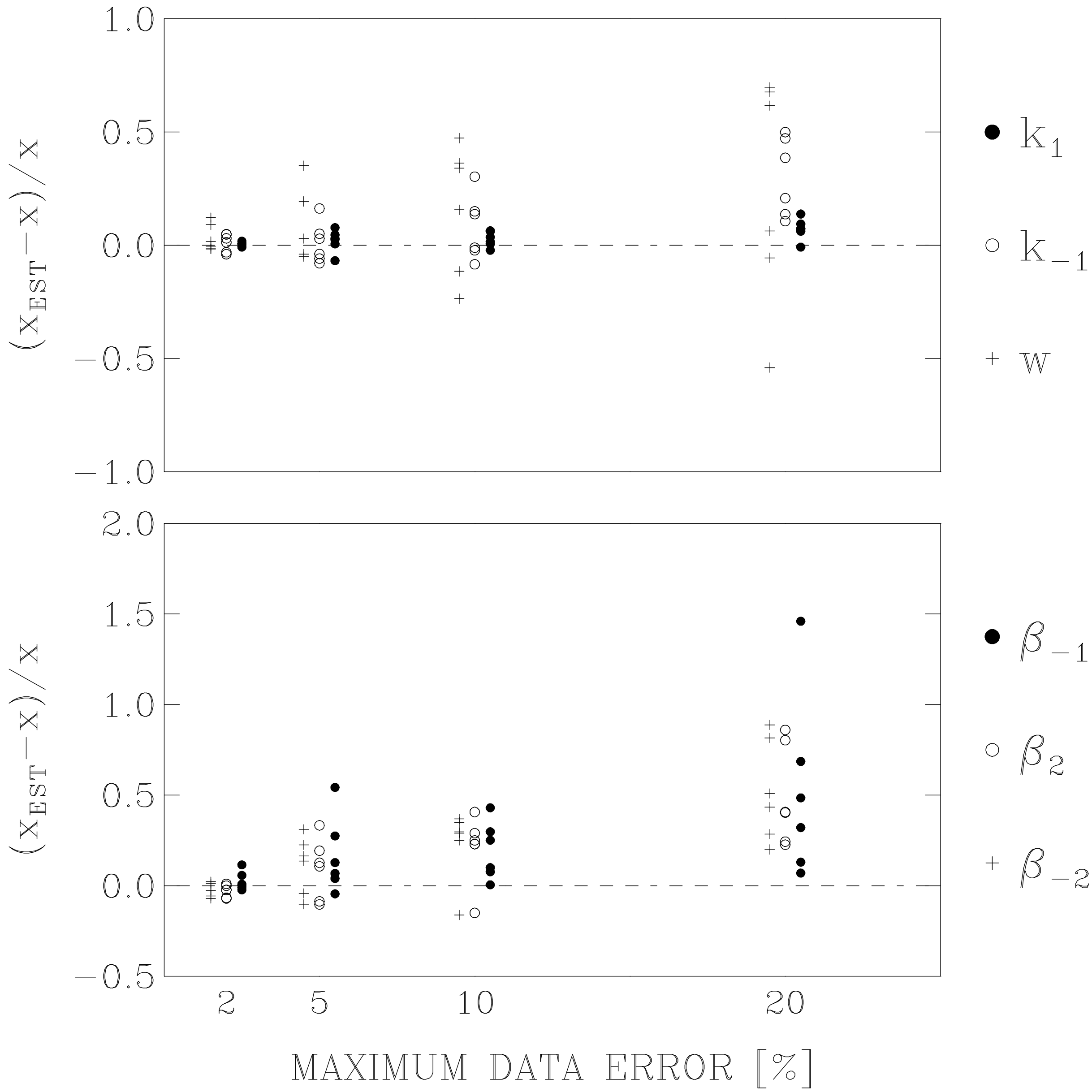

Figure 8: Effect of maximum data error on the accuracy of the rate constants of Th and particle cycling estimated by inversion. The accuracy is measured by the difference between the estimated value and the actual value, divided by the actual value.

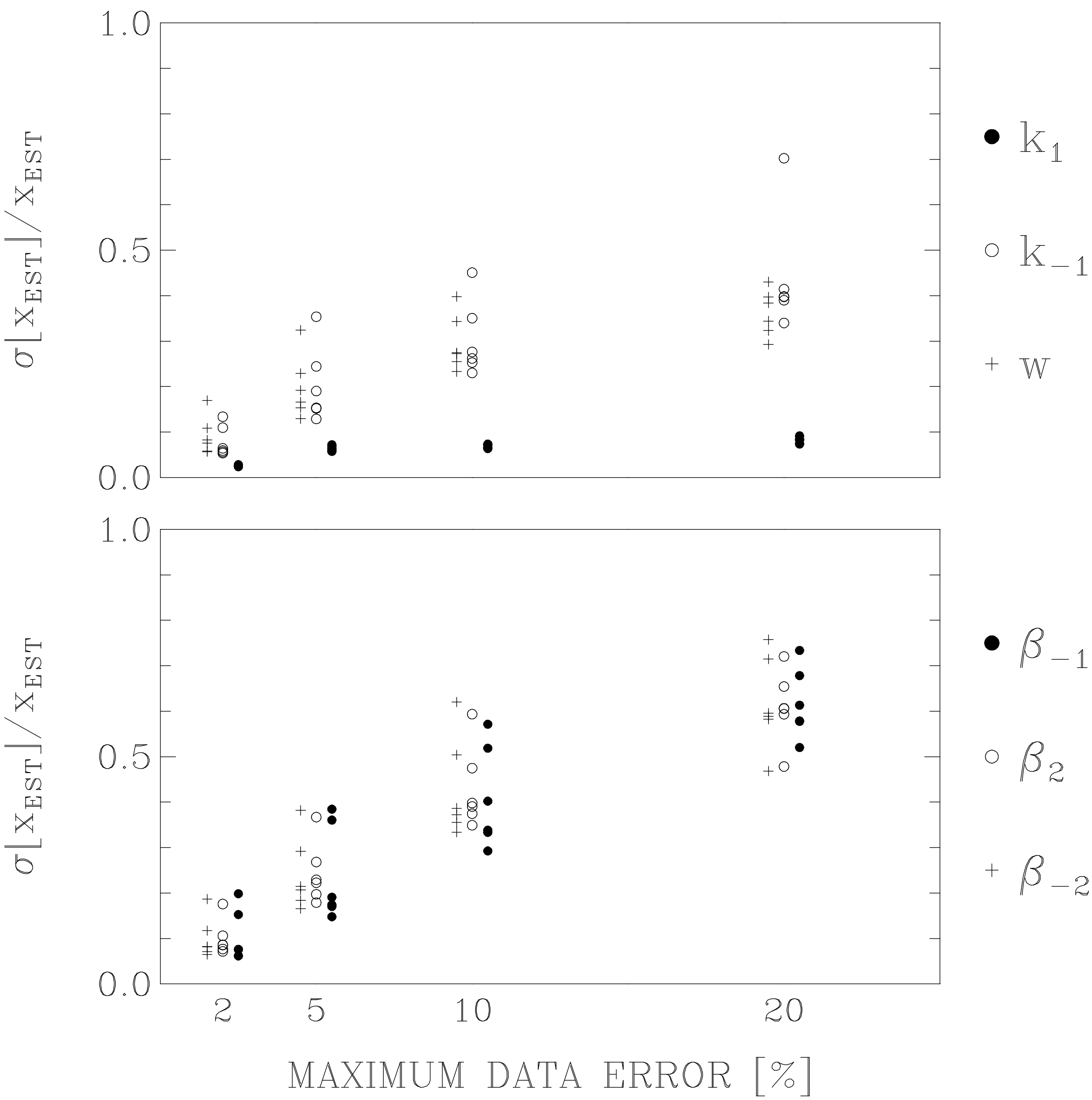

Figure 9: Effect of maximum data error on the precision of the rate constants of Th and particle cycling estimated by inversion. The precision is measured by the ratio between the standard deviation of the estimated value and the estimated value.

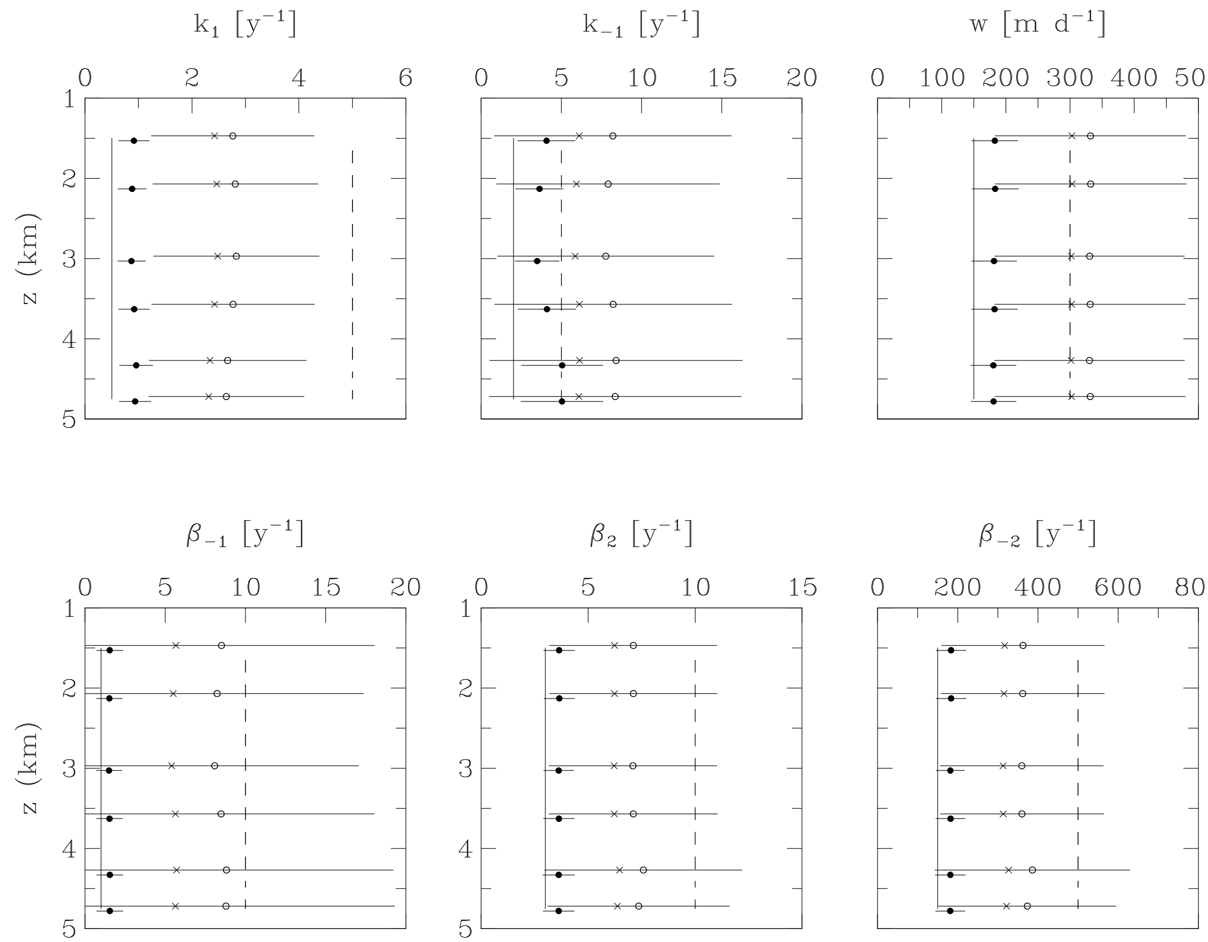

Figure 10: Rate constants of Th and particle cycling estimated with varying model errors. The vertical solid lines indicate the values used to generate Th and particle data. The vertical dashed lines indicate the prior estimates assumed in the inversions. The solid circles with horizontal bars show the means with their errors estimated in an inversion where $p = 0.1$. The open circles with horizontal bars (crosses) show the means (medians) with their errors estimated in an inversion where $p = 1$. In both inversions, the data have no error and are available at all depths. The rate constants estimated by inversion are shown at six of the pumping depths at GEOTRACES NA deep stations.

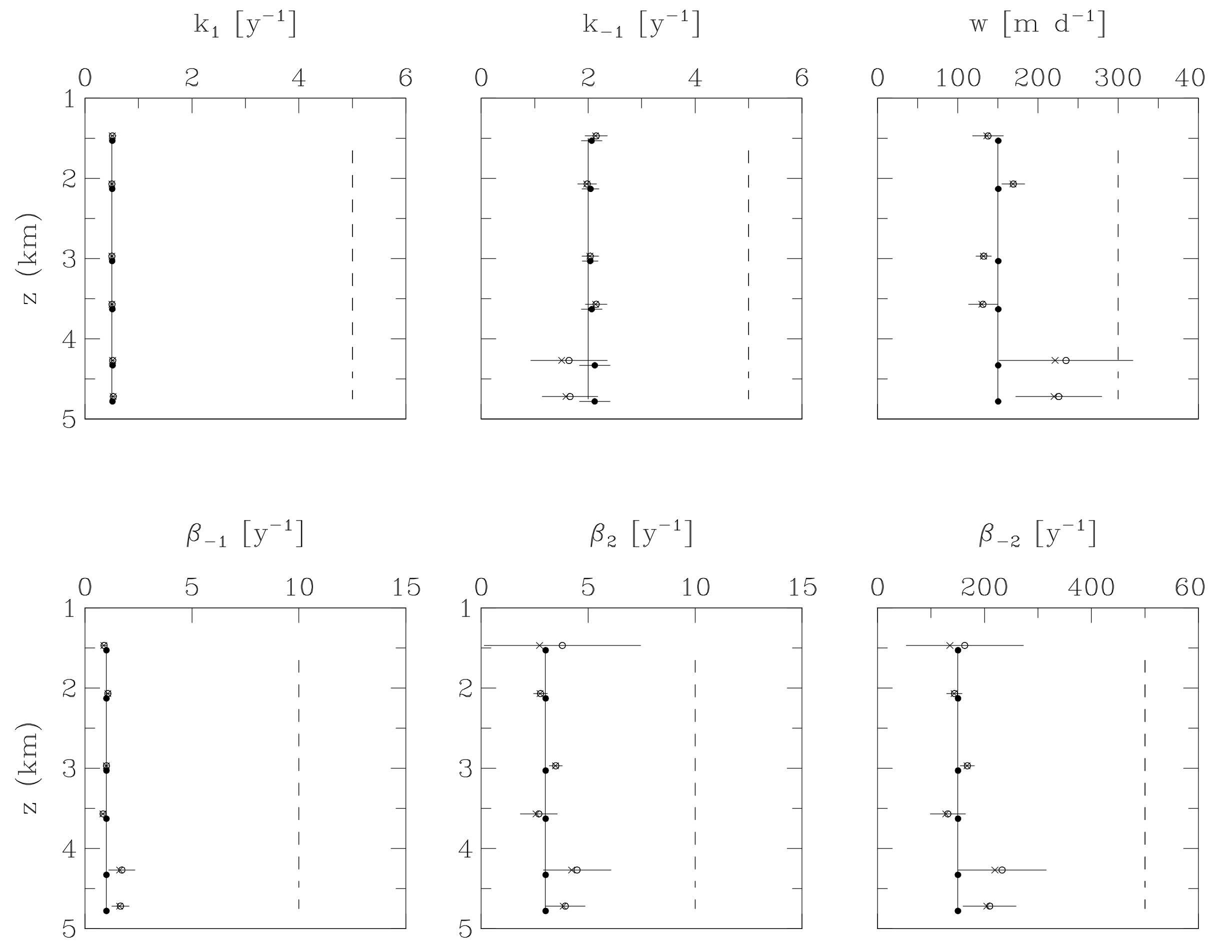

Figure 11: Rate constants of Th and particle cycling estimated with varying sampling schemes. The vertical solid lines indicate the values used to generate Th and particle data. The vertical dashed lines indicate the prior estimates assumed in the inversions. The solid circles with horizontal bars show the means with their errors estimated in an inversion where data are available at all depths. The open circles (crosses) with horizontal bars show the means (medians) with their errors estimated in an inversion where data are interpolated or extrapolated. In both inversions, the data have no error (except in the second inversion where extrapolated values have a relative error of 1) and the factor for model errors $p = 0.01$. The rate constants estimated by inversion are shown at six of the pumping depths at GEOTRACES NA deep stations.

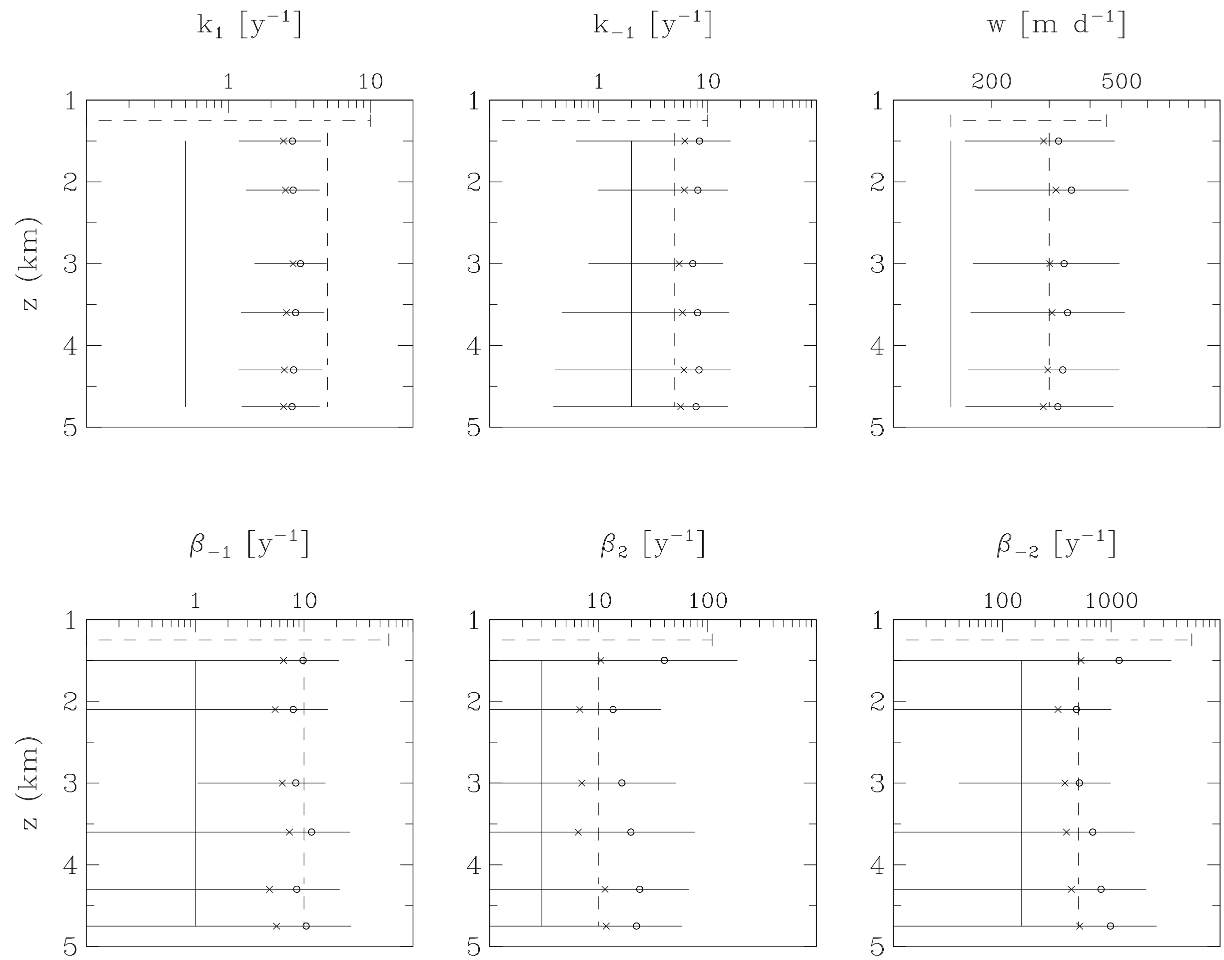

Figure 12: Rate constants of Th and particle cycling estimated in the presence of data errors, model errors, and limited sampling. The vertical solid lines indicate the values used to generate Th and particle data. The vertical (horizontal) dashed lines indicate the prior estimates (their errors) assumed in the inversions. The open circles (crosses) with horizontal bars show the means (medians) and their errors estimated in an inversion where (i) the errors and depths of the measurements would be those at GEOTRACES NA deep stations and (ii) the factor for model errors $p = 1$. The rate constants estimated by inversion are shown at six of the pumping depths at these stations.

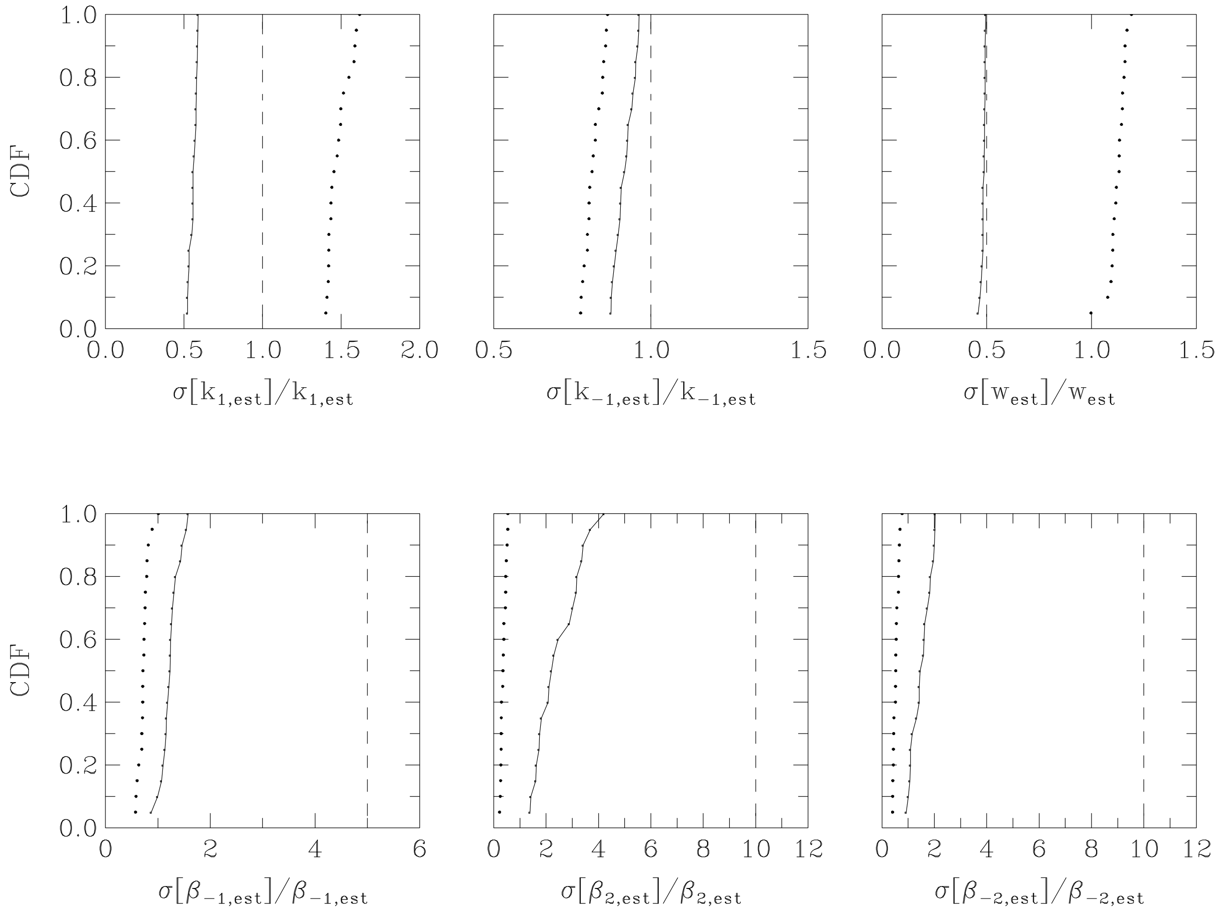

Figure 13: Cumulative distribution function (CDF) of the relative precision of the rate constants of Th and particle cycling, which are estimated in the presence of data errors, model errors, and limited sampling. The relative precision is the standard deviation of the rate constant divided by the value of the rate constant. The dashed (solid) line is the CDF for the prior (posterior) estimates. Also shown is the CDF of the difference between the estimated and actual value, divided by the standard deviation of the estimated value (dotted line). Note that the CDFs for the posterior estimates are based on values at all depths of the model grid.

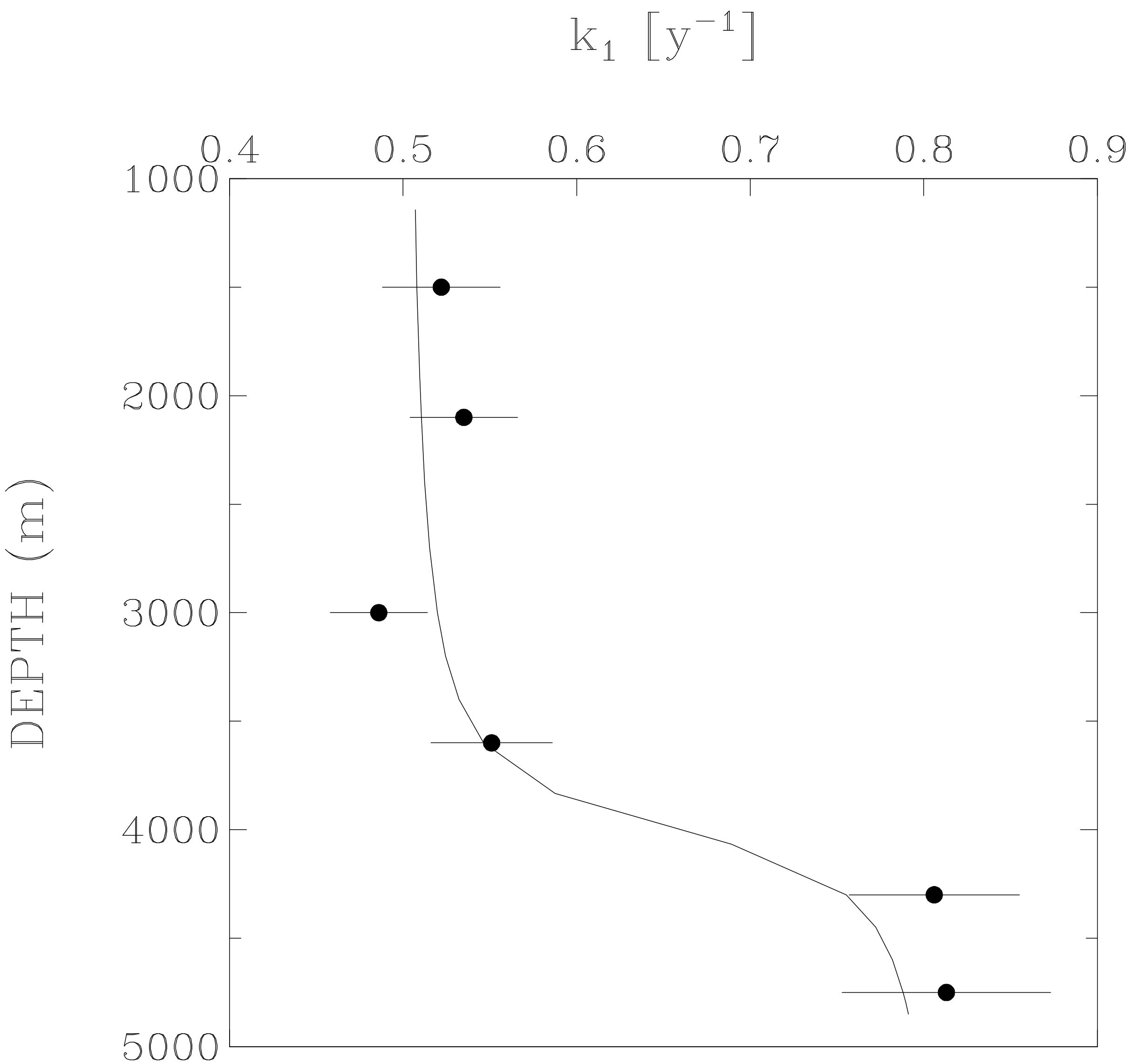

Figure 14: Recovery of vertical variations in the rate constant of Th adsorption. The solid line indicates values used to generate Th and particle data. The solid circles with horizontal bars show the means with their errors estimated in an inversion where the data have a relative error of 5%, they are available at all depths, and model errors are very small ($p = 10^{-5}$). Note that the values estimated by inversion are shown only at some of the pumping depths at GEOTRACES NA deep stations.

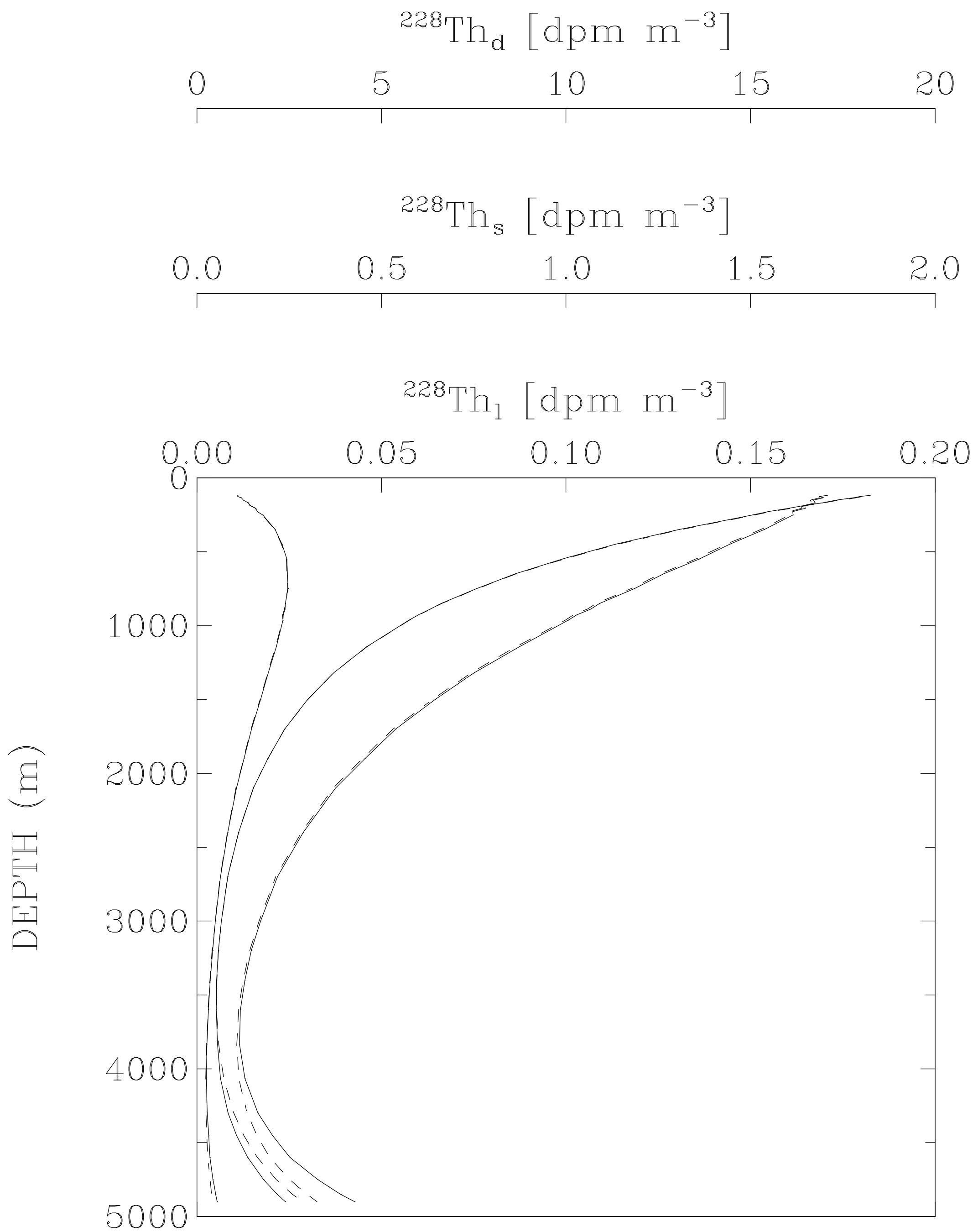

Figure 15: Vertical profiles of ^{228}Th activity in the dissolved phase (upper horizontal axis), the small particles (middle axis), and the large particles (lower axis). The ^{228}Th activities that are obtained by numerical solution with uniform (variable) rate of Th adsorption are shown by dashed (solid) lines (left most lines for large particles, middle lines for the dissolved phase, and right most lines for small particles).

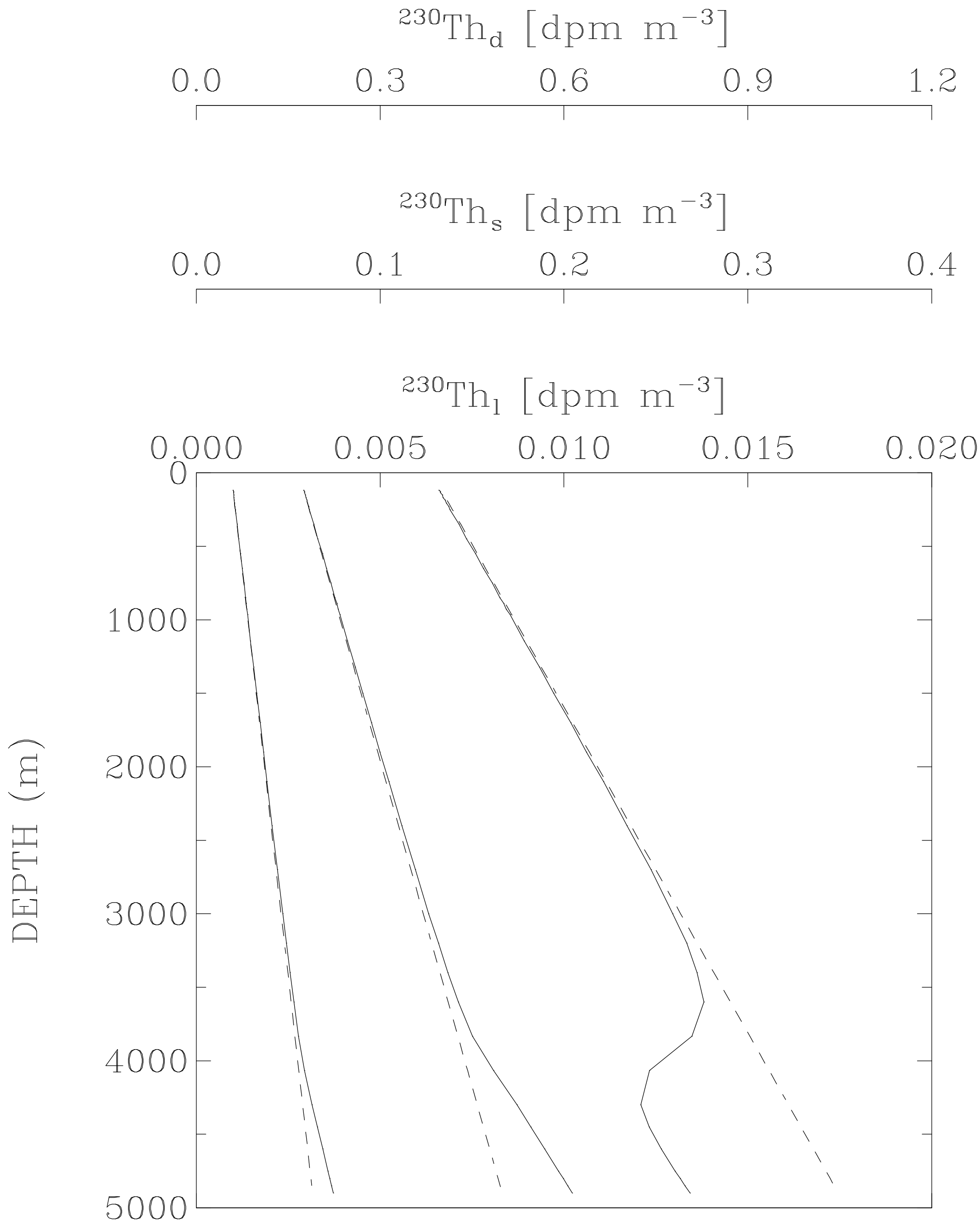

Figure 16: Same as Figure 15 but for ^{230}Th (left most lines for large particles, middle lines for small particles, and right most lines for the dissolved phase).

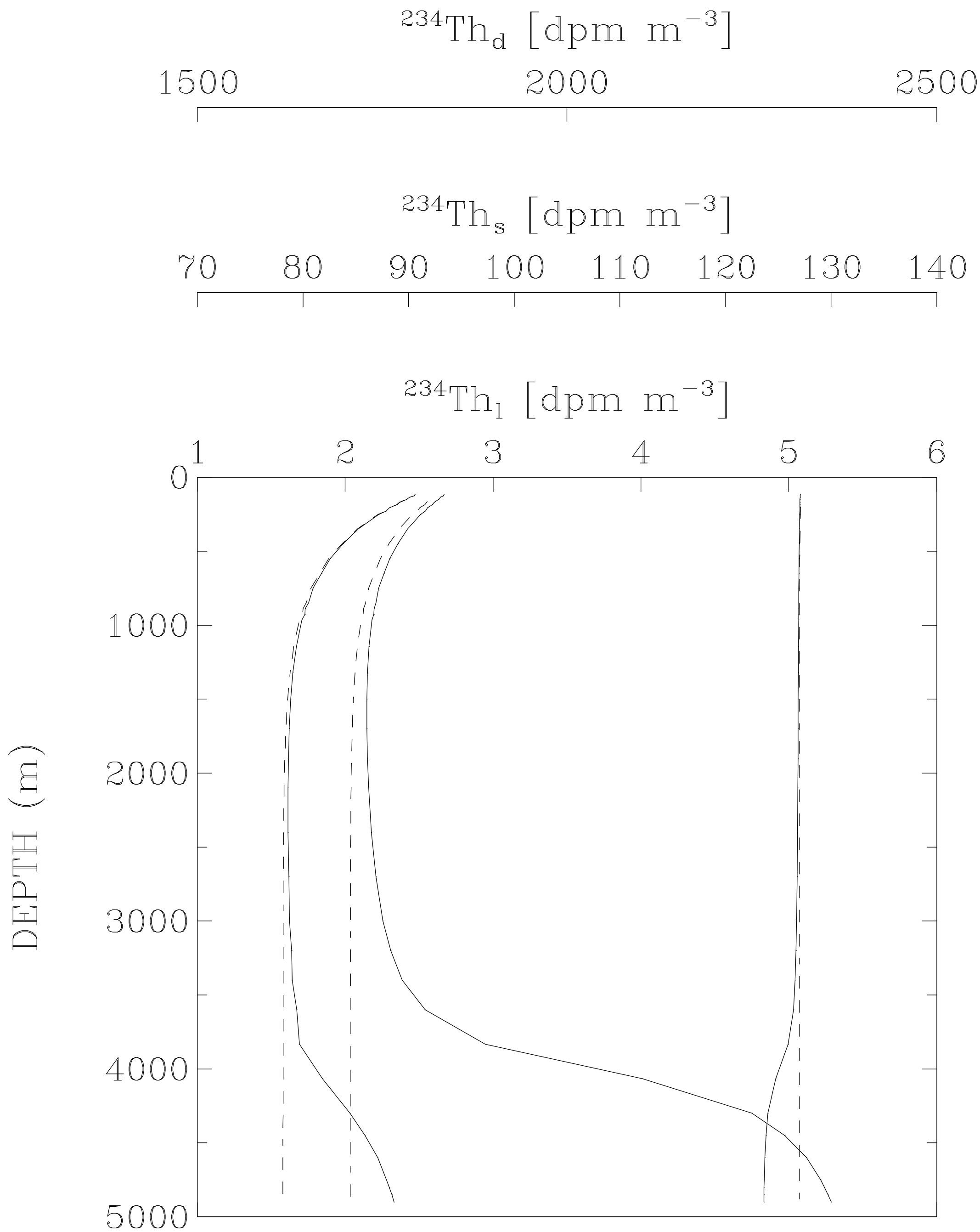

Figure 17: Same as Figure 15 but for ^{234}Th (left most lines for large particles, middle lines for small particles, and right most lines for the dissolved phase).

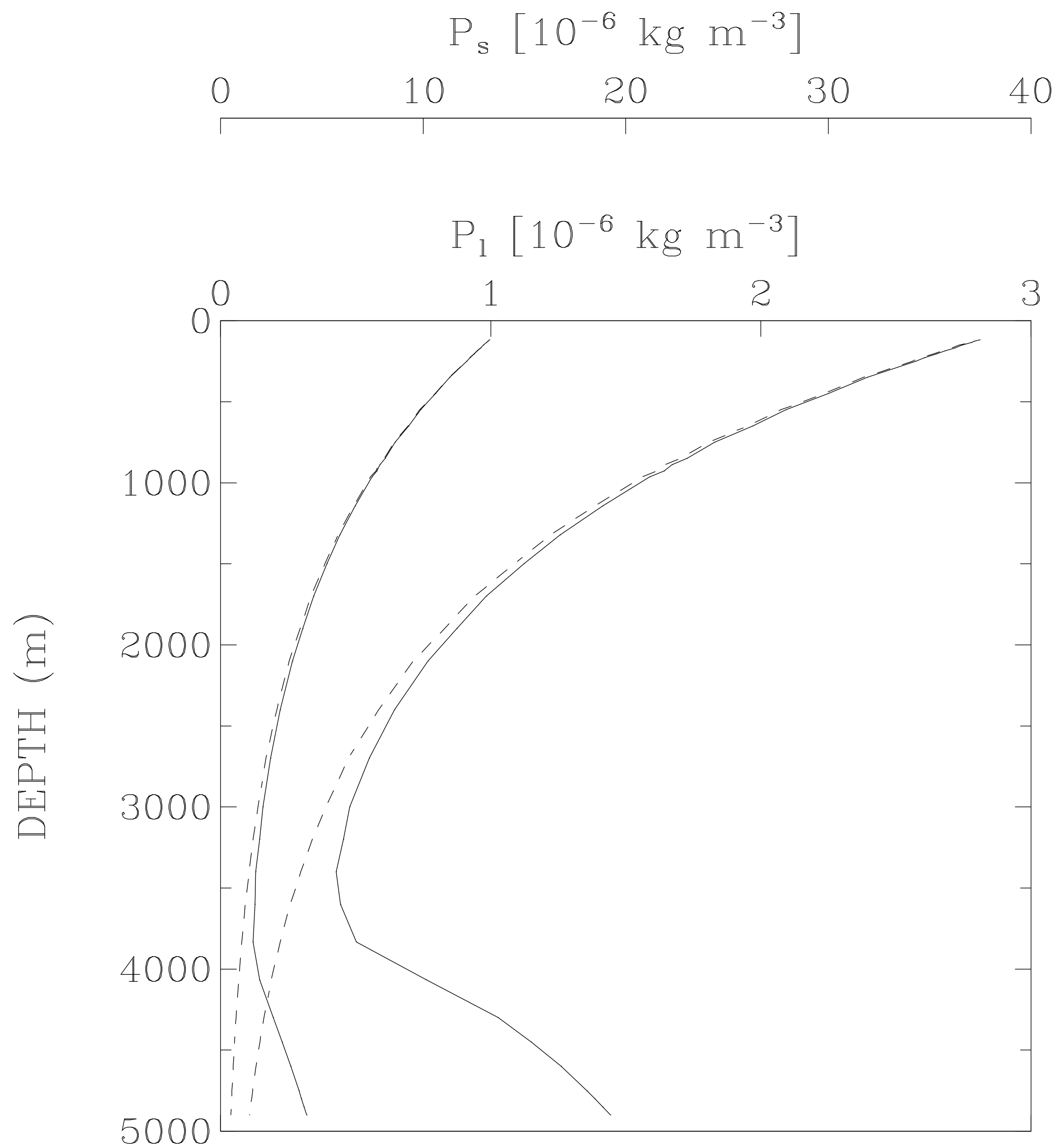

Figure 18: Same as Figure 15 but for the concentration of particles (left lines for large particles and right lines for small particles).

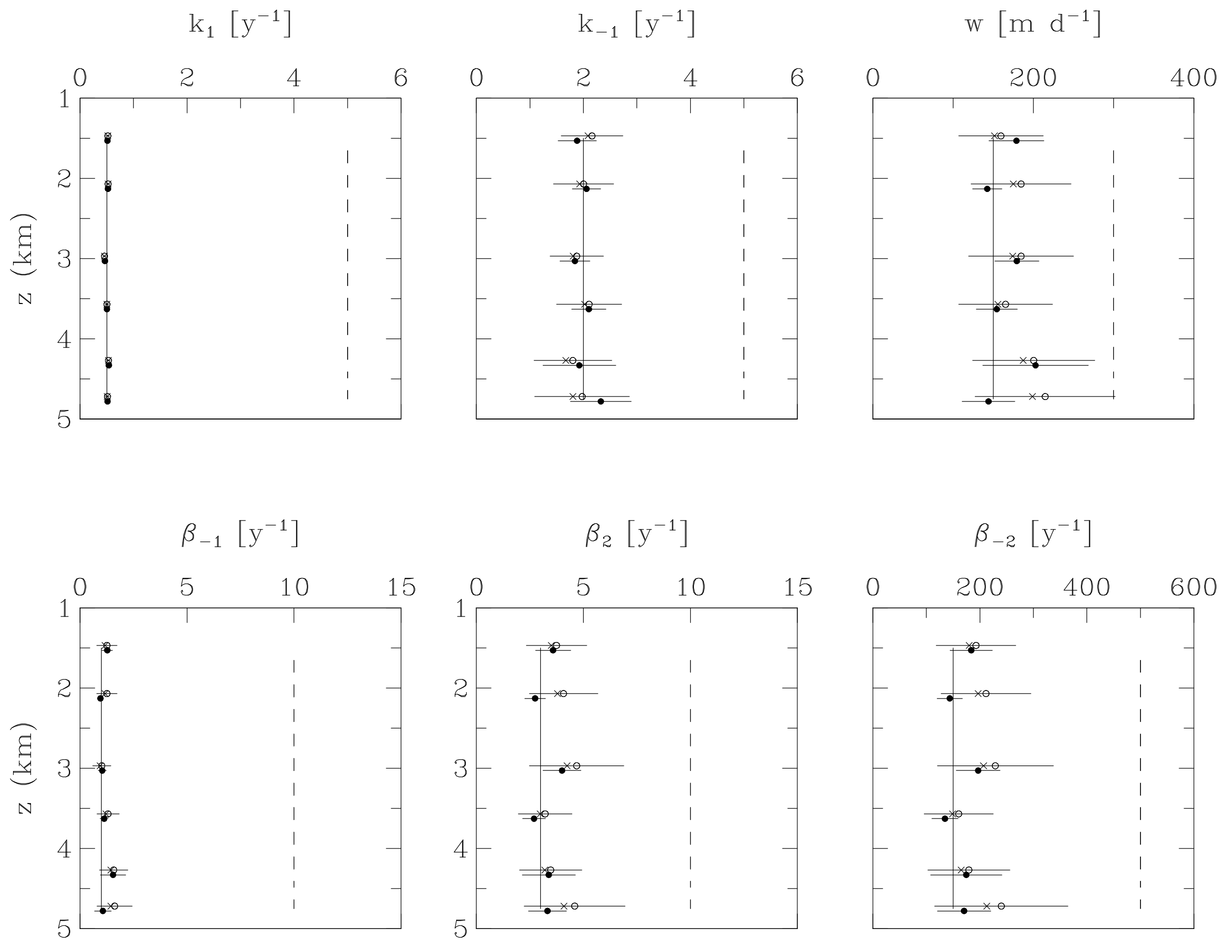

Figure 19: Rate constants of Th and particle cycling estimated with varying errors in the ^{228}Th equations. The vertical solid lines indicate the values used to generate Th and particle data. The vertical dashed lines indicate the prior estimates of the rate constants assumed in the inversions. The solid circles with horizontal bars show the means with their errors estimated in the reference inversion. The open circles (crosses) with horizontal bars show the means (medians) with their errors estimated in an inversion with a relatively large error for the ^{228}Th equations ($p = 1$). In both inversions, the data have a relative error of 5% and are available at all depths. The rate constants estimated by inversion are shown at six of the pumping depths at GEOTRACES NA deep stations.

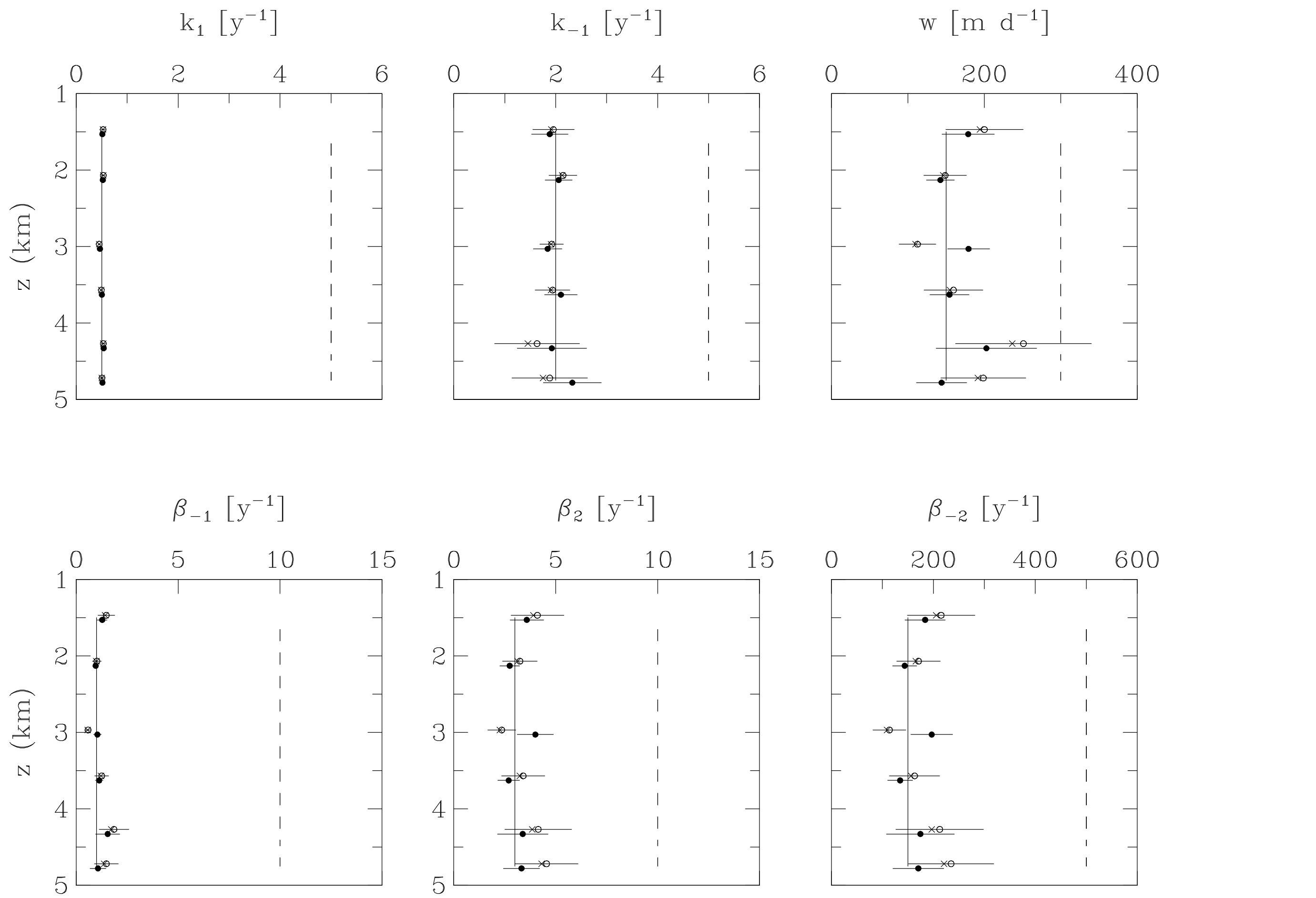

Figure 20: Rate constants of Th and particle cycling estimated with or without local ^{228}Ra data. The vertical solid lines indicate the values used to generate Th and particle data. The vertical dashed lines indicate the prior estimates assumed in the inversions. The solid circles with horizontal bars show the means with their errors estimated in the reference inversion. The open circles (crosses) with horizontal bars show the means (medians) with their errors estimated in an inversion where (i) ^{228}Ra activity is fixed to 2.4 dpm m^{-3} at all depths and (ii) the error in the ^{228}Th$_d$ equation is set equal to this value times the ^{228}Th radioactive decay constant. The rate constants estimated by inversion are shown at six of the pumping depths at GEOTRACES NA deep stations.